Julia Platzer, BSc

Optimization of sample preparation techniques for transmission electron microscopy of Al-Cu and Eco Mg alloys

MASTER THESIS

For obtaining the academic degree
Diplom-Ingenieur

Master Programme of
Advanced Materials Science

Graz University of Technology

Supervisor:
Ao.Univ.-Prof. Dipl.-Ing. Dr. techn. Gerald Kothleitner
Institute for Electron Microscopy and Nanoanalysis

Graz, February 2015

Abstract

This master thesis deals with the preparation of aluminium and magnesium alloys for high–resolution transmission electron microscope investigations (S/TEM).

Aluminium and magnesium alloys are widely spread material systems used in various industrial fields, like for instance in the automobile industry, as in Austria. One of the main reasons is due to the fact that aluminium on its own is three times lighter than steel. On the other hand, cell phone or notebook housings, to give an example, are often made of magnesium alloys, with magnesium having even a lower density than aluminium. Its alloys are used preferably for weight reduction, whenever possible and cost-effective.

The aim of this thesis was to find specific preparation recipes for these alloys, which have been modified and produced within the OPTIMATSTRUCT project. These recipes shall allow for representative investigations of their micro– and nano–structures by means of S/TEM and therefore contribute to the improvement of their overall properties.

The main methods used for the preparation were mechanical cutting and polishing, electrochemical polishing/thinning, ion polishing with argon or cutting with a focused gallium ion beam. All these methods are tested, combined, and compared to obtain optimal results.

The first visual characterization of the prepared samples was done with an optical microscope. Afterwards the samples were pre-characterized by conventional TEM in order to check their suitability for high–resolution investigations. These investigations were then performed on a high–resolution field-emission S/TEM microscope. The main criteria for a successful preparation were the presence of thin (10–60 nm), crystalline, and beam-stable areas.

The combination between electrochemical polishing at low temperatures (-10 to -20°C) and a final argon ion polishing at low voltage delivered the best result for aluminium alloys. The best samples for magnesium alloys have been produced by using only argon ion milling at low temperature (-20°C).

Kurzfassung

Diese Masterarbeit beschäftigt sich mit der Präparation von Aluminium– und Magnesiumlegierungen für Untersuchungen in einem hochauflösenden Transmissionselektronenmikroskop (S/TEM).

Aluminiumlegierungen und auch Magnesiumlegierungen haben ein großes Anwendungsgebiet in den unterschiedlichsten Industriebereichen. In Österreich werden sie vor allem in der Automobilindustrie eingesetzt, da reines Aluminium dreimal leichter als Stahl ist. Anderseits werden Magnesiumlegierungen auch unter anderem für Gehäuse von Mobiltelefonen und Notebooks eingesetzt, da Magnesium eine geringere Dichte als Aluminium hat. Deren Legierungen werden dann bevorzugt eingesetzt, wenn eine Gewichtsreduktion möglich und kostengünstiger ist.

Das Ziel dieser Masterarbeit ist es, gezielte Präparationsabläufe zu entwickeln, welche auf die Legierungen vom „OPTIMATSTRUCT“ abgestimmt sind. Durch diese Präparationsabläufe werden repräsentative Untersuchungen ihrer Mikro- und Nanostrukturen mittels S/TEM ermöglicht und tragen somit der Verbesserung der Gesamteigenschaften bei.

Folgende Methoden wurden hauptsächlich zur Herstellung herangezogen: mechanisches Schneiden und Polieren, elektrochemisches Polieren und Dünnen, Ionenpolieren mit Argon oder Schneiden mittels eines fokussierten Gallium-Ionenstrahls. All diese Verfahren wurden getestet, kombiniert und verglichen um optimale Ergebnisse zu erhalten.

Die erste Charakterisierung der hergestellten Proben wurde mit einem Lichtmikroskop durchgeführt. Anschließend wurde die Eignung der Proben für hochauflösende Untersuchungen mittels eines konventionellen TEM überprüft. Mit einem hochauflösenden Feldemissions-S/TEM-Mikroskops wurden die geeigneten Proben untersucht. Das wichtigste Kriterium für eine erfolgreiche Präparation ist das Vorhandensein von dünnen (10-60 nm), kristallinen und strahlstabilen Bereichen.

Die Kombination von elektrochemischen Polieren bei niedrigen Temperaturen (-10 bis -20°C) und einer kurzen Argonionenstrahl Behandlung bei niedriger Spannung lieferte das beste Ergebnis für die Aluminiumlegierungen. Die beste Probe der

Magnesiumlegierung, wurde mittels einer Argonionenstrahl-Präparation bei niedriger Temperatur (-20°C) erzielt.

Acknowledgments

First of all I want to thank Ferdinand Hofer and Gerald Kothleitner for the possibility to write my master thesis at the Institute for Electron Microscopy and Nanoanalysis.

I would like to express my gratitude to Mihaela Albu, who supported me with all of her possibilities during the whole time of the master thesis. Without her input, remarks and our discussions this master thesis would not be possible.

A lot of support and input came also from Martina Dienstleder and her immense knowledge about preparation of specimens.

The laboratory group with Margit Brunegger, Manuel Paller, Daniel Schreiner and Jakob Schaller helped me during the preparation experiments, whenever a problem occurred or company needed. I could also rely on the help and assistance of Claudia Mayrhofer, Ilse Letofsky-Papst and Angelika Reichmann.

Special thanks also to the whole team of the institute by offering so much support, practically and mentally.

Furthermore I am thankful to my family, friends and Michael, who have supported me throughout my master degree and the whole master thesis process. I got enormous backing and patience from all of you.

Content

1. Introduction/Motivation

Specimen preparation is one of the most important and critical steps in transmission electron microscopy. Without a proper preparation of the samples, high-resolution imaging, possibly also including all the other analytical possibilities of an electron microscope, would be meaningless. Even for light optical microscopy, the surface preparation is crucial for material analysis. [1, 2, 3]

The objective of the preparation process optimization is to obtain a suitable specimen for TEM work. This “ideal specimen” should have large planar areas, which are electron transparent at thicknesses lower than 100 nm. These areas furthermore should be representative of the bulk sample, i.e. without deviations from material, structure, and chemistry. It should also be stable under the electron beam, robust against oxidation and other environmental influences. Other desired properties for TEM work would be conductivity, surface cleanliness, and being non-magnetic. The closer a specimen resembles this ideal, the higher the quality and the better the investigation results that can be expected. [1, 2, 3]

The aim of this master thesis is to improve the preparation of aluminium and magnesium alloys for high–resolution (scanning) transmission electron microscopy (S/HRTEM) investigations. The main criteria of the preparation were the provision of thin, large-area, and crystalline areas with no significant change in its original structure. The focus was put on the optimization of the promising electrochemical polishing process, offered by a “TenuPol-5” device from the Struers company. Other possibilities, such as argon milling and focused ion beam, have been considered in this thesis as well. Some subsequent treatments (He/Ar plasma cleaning) and difficulties, especially in the case of magnesium alloys, are also discussed.

As already mentioned, the thesis concerns two alloy–systems, aluminium and magnesium. These materials are central in a project called COIN OPTIMATSTRUCT funded by FFG [4]. The importance of these alloys is given by the enormous application possibilities. Most importantly, they are used in cases where light materials are preferred, substituting other materials. Compared to steel, aluminium and magnesium are lighter and have lower densities. Magnesium is four times lighter than steel und one and a half times lighter than aluminium [5]. Especially in

transportation (cars, planes, boats, etc.) weight reduction is an important goal, driving the new development and improvement of novel aluminium and magnesium alloys. Since material properties such as creep resistance, temperature dependence, fatigue, corrosion or wear resistance are strongly influenced by the material's micro– and nanostructure and chemistry, a profound knowledge of the crystal structure, present defects or precipitation is mandatory. Ongoing material design and the improvement of material properties hence require investigations at the micro to nano-scale, which is only possible, if well prepared S/TEM specimens are available.

2. Specimen preparation for electron microscopy

2.1 General preparation

Depending on the information sought about the material, a few questions need to be addressed first:

1.) What kind of specimen is being dealt with and how is the physical presence of the sample (bulk, powder, or nano-crystals in liquid…)?
2.) What kind of information should be obtained? Chemical composition, surface information, crystallographic structure or physical properties.
3.) Which microscopy or spectroscopy method on which system will be used? Optical microscopy (OM), scanning electron microscopy (SEM), transmission electron microscopy (TEM), high resolution TEM (HRTEM), scanning TEM (STEM), electron energy loss spectroscopy (EELS), etc.

Table 1 gives a general overview on common microscopic techniques, specimen preparation and their typical usage [6].

Table 1: Common Microscopic Techniques and Sample Preparation Concerns/Aspects [6]

Common Microscopic Techniques	Properties	Sample preparation
Optical microscopy (OM) **Reflection** **Transmission** **Phase contrast** **Polarized light**	Surface and internal microscopy, crystallographic identification of particulates. Max. magnification ~1000x	Polish and etch one side for reflection modes. Some thinning for transmission mode.
SEM	Surface and internal morphology with 1000 Å or better resolution. Special techniques to characterize semiconductor and magnetic devices.	Polish and etch one side (apply coating if required).
TEM **STEM** **HRTEM** **Analytical electron microscope**	Internal nanostructure. Some case of surface structure if using replicas. Spatial resolution 2-5 Å. Phase determination (often with stained specimens) capability. Crystallographic information from ~40000Å^2 area.	Very critical, ultrathin specimens needed.

During the preparation steps the structure might be influenced by mechanical, ionic, or chemical actions. How these factors can influence the material and the obtained information of the investigations is visible in chapter 2.3. [1]

Figure 1 and 2 depicts the preparation steps. Basically, starting with a bulk material, the first step is to cut the sample to a specific size with a cutting wheel or a wire. These wires and wheels contain abrasive grains, with different sizes and hardness. Which kind of wheel or wire with the corresponding abrasive is being used, depends inter alia on the hardness of the specimen or on the preparation step. The final cutting size depends on the microscope, for which it is prepared. For SEM a few centimetres are acceptable, but specimens for TEM eventually have the size of a few millimetres and they are also very thin. Basically, in order to avoid any alterations of the structure of the specimens, special saws should be used. Normal ones can damage the surface up to 200 µm inside the specimen. The usage of special preparation saws with the right settings can reduce the damage in the surface up to 1 µm or less. These saws can have rotating blades, with a diameter of 10 µm or are string saws with embedded diamonds. Another characteristic is the lubricant, being either alcohol, oil or water, which can also act as a cooling agent. These saws allow a specimen thickness of about 100 µm. The use of an acid string saw can reduce the mechanical damage and the deformation. Through this acid or etching agent, a chemical reaction occurs with the material, by means of this reaction, the sample is being cut. However, if the material is inert or too reactive this practice is not possible. [2, 6]

After the slicing, the surface has to be grinded and polished. This sample preparation technique is useful for SEM and optical microscope investigations.

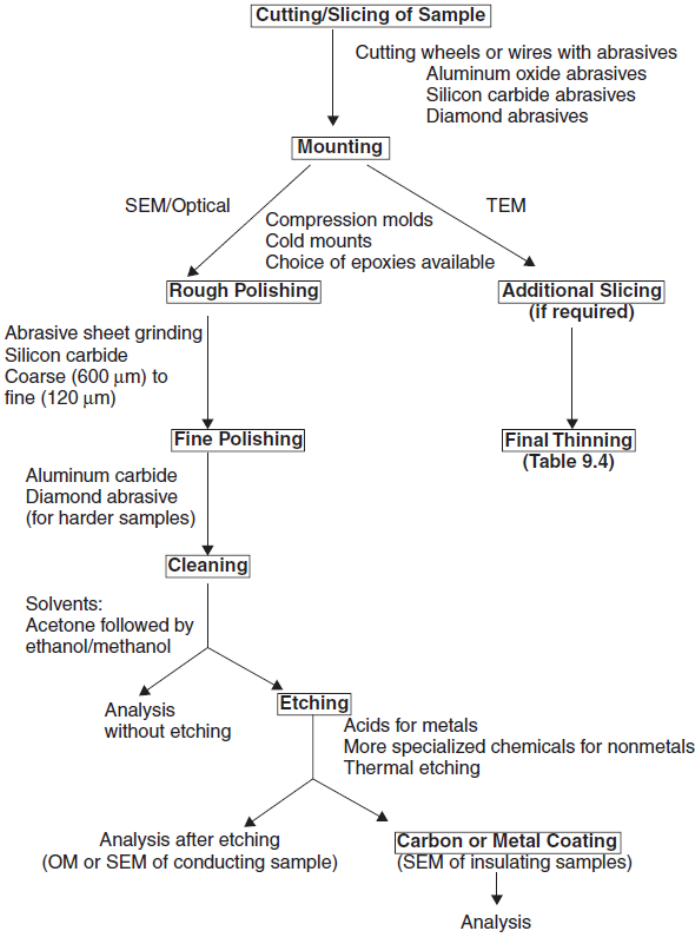

Figure 1: Basic steps for specimen preparation for SEM and LOM microscopy [6]

For surface analysis in SEM grinding and polishing is crucial. For this step of preparation the specimens are compression moulded or cold mounted in a polymer mould. For grinding, different abrasive papers with different grits are used. In order to reduce the surface deformation, the abrasive papers are finer from step to step. Main abrasive materials are silicon carbide (SiC) at abrasive papers, aluminium oxide suspensions (Al_2O_3) and for very hard materials diamond paste. After this step, the surface should be flat, smooth, and no scratches should be visible. After cleaning the surface with action, ethanol, or methanol the specimen can be used for analysis. [6]

For further investigations, the specimen has to be treated either with chemical or thermal etching, or with a combination of both. By etching the surface, the lowest-energy surface is uncovered. Grain boundaries and other structural defects are exposed and through that, a contrast is induced. The contrast shows different crystallographic orientation of phases, which altered differently. [6]

For SEM investigation the specimens should be conductive. Non-conductive specimens need a thin coating layer. The most popular coating is carbon, because it does not influence x-ray measuring since its signal is almost undetectable. Other coating possibilities involve metals, such as gold or less commonly organic layers. Typical methods of coating the surface are thermal evaporation and sputtering. [6]

As mentioned above, cutting as well as all the other steps can induce or influence microstructural changes or artefacts, which cannot always be annihilated by heat treatments or other techniques. This is important to keep in mind when analysing the specimens at the microscopes. [1, 2, 6]

In the next chapter, TEM preparation will be explained in more detail.

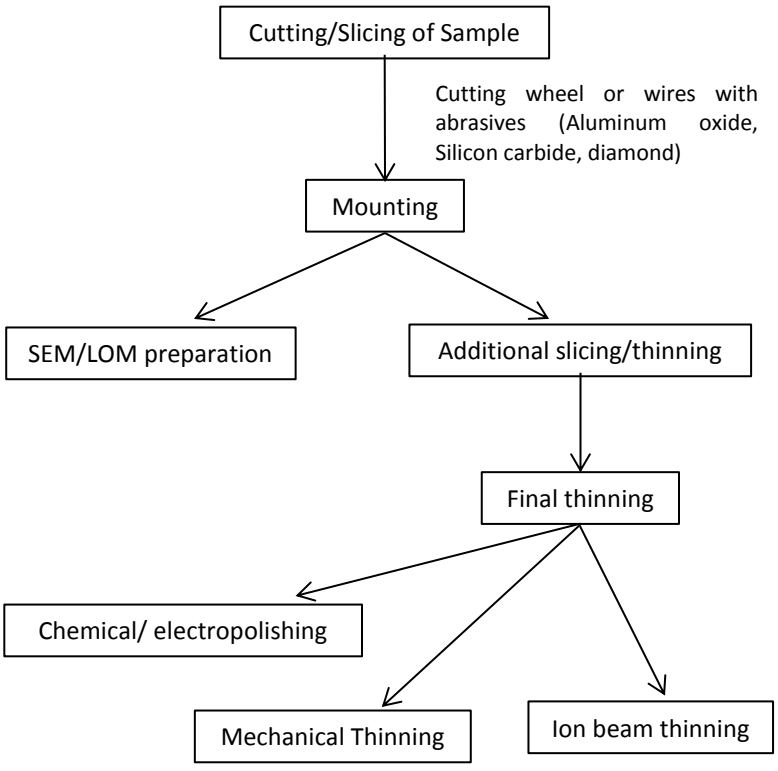

Figure 2: Basic steps for specimen preparation for TEM microscopy (analogue to figure 1)

2.2 Sample preparation for transmission electron microscopy

Sample preparation for transmission electron microscopy differs from the former, as it aims to produce thin, wide-area regions with a thickness of less than 100 nm or even 50 nm for high-resolution investigations. This is just a rough number, because heavier elements often demand even thinner samples for the same conditions. [1, 6]

The first step in preparation is the same as mentioned in the chapter 2.1 and it can also be seen in figure 1. [6] This chapter will concentrate on preparation of bulk materials, which are self–supporting. The other group requires a support grid, usually made of copper, but also could be gold, nickel, or beryllium. [7] The latter group is discussed in 2.2.3, where microtomy will be explained.

The specimen should be shaped such that it fits into the TEM–sample holder. It can be disc-shaped, wedge shaped and, if FIB prepared, also lamellar. The most common geometry for argon milling or electropolishing is a disc shape, with a diameter of approximately 3 mm, which fits directly into a TEM holder. [2]

After the initial cut, the material often has a thickness between 100 to 300 µm. From these slices 3 mm discs are then generated. For this procedure, a disc punch is typically used. After the sheet is placed right in front of the stamp and applying a force, the disc is punched out with low damage away from the border. Shear transformation can occur in some materials at this step mostly at the outer rim. For brittle materials, an ultrasonic disc cutter is used. [2]

Throughout this work the disc punch was used for the preparation of aluminium and magnesium alloys, so other possibilities will not be explained further.

Pre–thinning is required, when the thickness of the sample is not suitable for the final thinning. It can be done via mechanical polishing, mechanical or chemical dimpling, which are, apart from the chemical thinning, abrasive techniques. During the mechanical polishing, abrasives with decreasing grain sizes are taken, having impact on the smoothness of the surface. With this technique, the whole sample is evenly thinned and smoothed, whereas with the dimpling method, only the middle of the sample is thinned. With the help of a special tool, featuring a defined radius, a pan with a special curvature is created. The same abrasive pastes are used, as with the mechanical thinning method. Overall, a thickness in the middle of the sample of 50 to

80 µm or even less is aimed for, in order to reduce the final thinning time. Chemical dimpling uses a jet, of an etching solution which impacts the sample. [1, 2, 7]

The final thinning step, after pre–thinning, can be divided into two main groups, chemical and electropolishing and ion beam thinning. These two techniques together with microtomy (producing directly investigable specimens) are explained next. [6]

2.2.1 Chemical and electropolishing

The first patent application for the electropolishing process was filed in 1930 and, it has been continuously developed since then [7]. Thin foils are produced, with little to no mechanical damage, through (anodical in the electro chemical case) dissolution of the material and spatial removal of the dissolvent. The requirements for the solvent are: Firstly, it should be oxidizing (acid or base), secondly, it should control the passivation layer (regulates the dissolving rate) and third, it should form a viscous layer close to the surface of the specimen, where the levelling of the surface happens. [1, 2, 6, 7]

Chemical polishing, in its simplest way, means holding the sample directly into the electrolyte, so that a reaction can start at the typically thinnest spot (mainly created by pre–thinning). It is used for non-electrically conductive samples, e.g. Oxides or glasses. Furthermore, the reactivity of electrolytes can be controlled by adapting the temperature [1, 2, 6].

The main difference between chemical and electropolishing is the additional application of an electric potential during thinning. According to Landolt 1987 [8], one can differentiate between macro- and microsmoothing stages. Macro smoothing denotes the smoothing of the rough surface, happening at the thick viscous layer. Whereas micro smoothing brightens the surface at a finer level and takes place at a thin film beneath the other one. [2, 8]

For good thinning results after polishing, the right electrolyte, potential, flow rate and temperature should be set, often requiring repetitive action. For instance when the potential is too low, etching occurs whereas if the potential is too high, pitting can start. Figure 3 shows an ideal current–potential curve, analogues to Petzow [9]. Between point A and point B etching occurs, because dissolution happens without

the formation of a stable viscous layer. After formation of this layer, the best polishing regime is between C and D. After point D, gas develops and the protecting film is interrupted and pitting of the surface starts. While the specimen still features holes and transmissive areas, large and thin areas are hard to find. [2, 9]

Control over temperature during the polishing is also an important factor. The sample temperature can rise up to temperatures due to power dissipation, conductivity of the electrolyte and specimen sometimes. Even if materials do not undergo phase transitions at these temperatures, chemical changes can take place due to enhanced diffusion, altering composition and structure. Working at low or negative temperatures while stirring the electrolyte, can keep the specimen temperature down. [2]

A of this kind is called TenuPol 5 from Struers. [10]

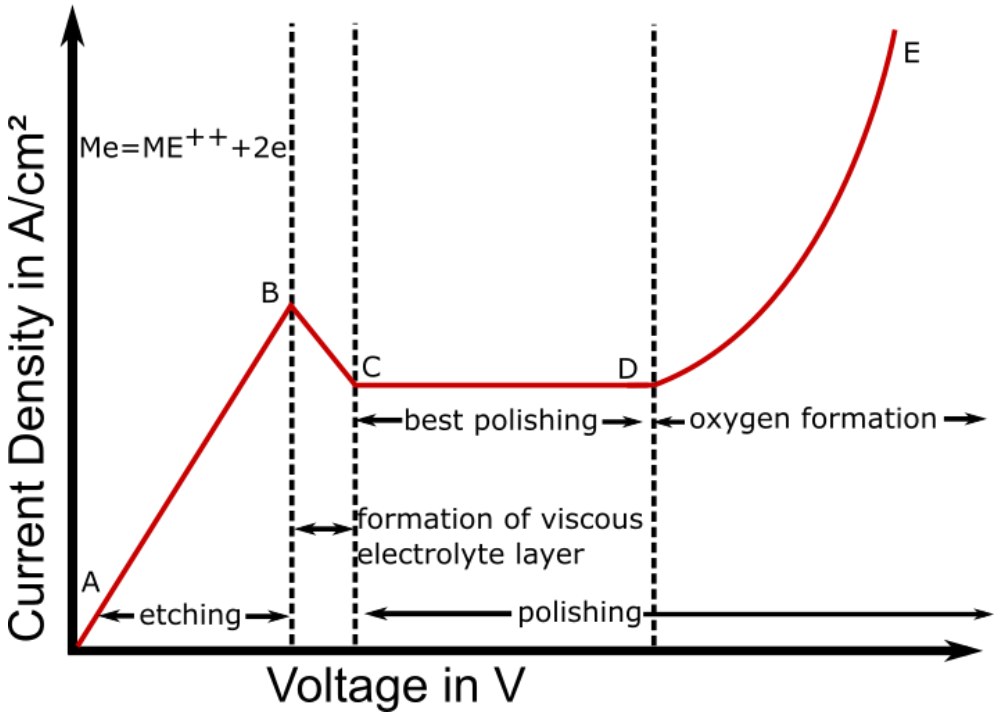

Figure 3: Characteristic current density – voltage curve, modified from Petzow, figure1.5.3-2 [9]

2.2.2 Ion beam thinning

This method, introduced during the 1960s, uses an ion beam for the removal of the material from the specimen surface, generated by electrical discharge. The beam is focused onto the surface of the sample with ion guns, leading to an atomic removal of material. The sputtering rate depends on the acceleration voltage, the relative mass of the ions, the angle of incidence of the ions, the atomic species, and the crystallinity of the specimen. [1, 2, 6]

At low ion energies (10–40 eV) hardly any atoms will be removed reaching a rate of 1–50 atoms per ion at energies between 2–30 keV. With energies between 1–5 keV and at a low incident angle, therefore the removal is very slow and layer–by–layer atomic erosion occurs. When carried out gently, this process allows removing contamination from the surfaces, and to clean and reduce amorphous layers from crystalline specimens. At higher energies and higher beam currency, thinning at the macroscopic level occurs. However if the energy is too high, the removal rate can approach zero, because atomic implantation happens rather than the removal of atoms. [1, 2, 6, 7]

For this process, mainly argon gas is used, which reaches a penetration depth of a few nanometres, depending on the exact conditions. As long as no reactive ion thinning is done, the gas should be inert (that means also that no chemically interaction with the sample occurs), as heavy as possible, and it should be atomic and not molecular. Reactive ion thinning happens with gases, so that the process is assisted by chemical reactions that take place on the surface. [1, 2, 6, 7]

The biggest advantage of ion beam thinning is that it works for almost every bulk material and even for embedded powders, particles, and fibres. Problems such as sample heating can occur, but especially newer devices, feature an internal cooling system to keep the temperature rise moderate. [1, 2, 6, 7]

2.2.3 Ultramicrotomy

Ultramicrotomy was originally designed for cutting soft biological samples. Nowadays, also inorganic materials, such as polymers, paper or other engineered materials are prepared. Cutting ductile metals such as aluminium and copper, brittle ceramics and porous (but embedded) materials is also possible. Very soft materials or materials which are smearing at room temperature can be cut at a frozen state with liquid nitrogen being used as a cooling agent. [1, 2, 6, 7, 11, 12]

The method essentially produces very thin, already electron transparent slices of the samples by direct cutting with a knife made of glass (for softer materials) or diamond (for harder materials). The principal components besides the knife are a movable piston and a special mechanism to advance this piston. Specimens (often embedded in a resin when soft) are mounted onto this piston, and by an excentric movement, the specimen is brought over the knife, cutting the sample to a thickness, defined by its thermal or piezo-electric advancement. The knife initiates a crack at the sample, which is propagated further due to the prism shape of the tool. This thin slice drops directly onto an inert liquid on which it is floating until picked up with a sample grid. Even though with this technique no chemical change takes place, a massive mechanical compression happens and plastic deformation occurs. [1, 2, 6, 7]

2.2.4 Other techniques

In addition to the techniques relevant for this experimental work, some special methods like cross section thinning, wedge cleavage, and tripod polishing shall be mentioned for completion. [2, 6]

Tripod polishing denotes a pure mechanical thinning method down to electron transparency by means of finely tiltable device. This special set–up is used for specimens, which are non-metallic and often brittle (e.g. semiconductors). [6]

For crystalline samples wedge cleavage can be applied, due to defined crystallographic planes present along which the material can be easily split. Layered materials are suitable for this technique, too. The prepared wedges can be mounted onto a grid for direct observation under the microscope. [2, 7]

Cross section thinning is used, whenever interfaces or layered materials need to be investigated 90° perpendicular to the observation direction. [2, 7]

2.3 Preparation induced artefacts

In the following table (Table 2), artefacts, induced during the preparation, are listed. A specimen preparation without artefacts is hardly possible, so it is important to keep in mind what can happen to the sample and how the preparation process can influence the structure upon observation with a TEM. [1]

In the first column (1), the mechanical preparation–induced artefacts are listed. Column 2 refers to the ionic preparation–induced artefacts, column 3 to chemical preparation–induced artefacts and (4) to physical preparation–induced artefacts. Secondary thermal damages are not listed, but examples are fusion, phase transformation, loss of chemical elements, amorphization, and changes in distribution of the phases. [1]

Table 2: Table summarizing the various artifacts formed by the preparation techniques [1]

Mechanical preparation–induced artifacts	Ionic preparation–induced artifacts	Chemical preparation–induced artifacts	Physical preparation–induced artifacts
Deformation	Redeposition	Material displacement	Deformation
Material displacement	Implantation	Selective dissolution	Microstructural change
Material tearing	Vacancies	Compositional change	Segregation of liquid phases
Cracks	Dislocation loops	Microstructure change	
Fractures	Cavities	Change of molecular bonds	
Inclusions of abrasive grains	Fractures	Change of natural contrast	
Dislocations	Roughness	Protein reticulation	
Glide planes	Selective abrasion	Residues	
Twinning	Structural change		
Stain hardening	Microstructure change		
Selective abrasion			
Particle aggregation			
Roughness			
Structural change			
Microstructure change			
Crystal–network change			
Composition change			
Residues			

3. Material

3.1 Aluminium Alloys

The top ten of primary aluminium producing countries in 2012 were China, Russia, Canada, the United States of America, Australia, the United Arabic Emirates, India, Brazil, Norway and Bahrain. [13]

For the most part of the aluminium production the metal is used for metallurgy. Examples of its usage are casting and wrought products (i.e. aluminium based alloys), coatings for different metals (as prevention layers) and as a reducing agent for other metal–oxides and –fluorides. [14]

Aluminium can be used as an addition to other alloys or as an alloy itself and whenever combined with other elements, a wide range of properties can be achieved, leading to different applications. To increase strength, for instance, mainly copper, magnesium, manganese, silicon and/or zinc are added. The maximum solid solubility of these elements is 1.5 wt% in aluminium. Elements with less solubility (e.g. zirconium and titanium) can influence the structure, e.g. the as-cast grain size (increases yield strength). [14, 15]

Wrought alloys can be categorized into non-heat treatable and heat treatable which can be further classified into different alloy series. The classification of aluminium-alloys, according to DIN EN 573-3, is listed in the following table (Table 3) [15]. Whereas the alloy series 1xxx, 3xxx, 4xxx and 5xxx belong to the non–heat treatable alloys, the other series (except 8xxx) are heat treatable [16]. Table 4 gives an overview of the abbreviations of heat treatments and their meaning.

The three numbers, which are marked as XXX, have different significations. The first X specifies the variation of an already existing alloy, the second and the third are to identify the alloy. The three numbers only vary at the first series (1XXX), in which case, the first X denotes modification with or impurities of other elements. The last two XX, describe the purity of the aluminium over 99.XX % [17].

Table 3: Wrought alloy classification DIN EN 573-3 [15]

Alloy series	Main alloying element	Alloying elements
1XXX	Aluminium (Al)	Al >99%, unalloyed
2XXX	Copper (Cu)	Mg, Mn, Bi, Pb, Si
3XXX	Manganese (Mn)	Mg, Cu
4XXX	Silicon (Si)	Mg, Bi, Fe, Cu, Ni
5XXX	Magnesia (Mg)	Mn, (Cr, Zr)
6XXX	Magnesia – Silicon (MgSi)	Mn, Cu, Pb
7XXX	Tin (Zn)	Mg, Cu, Ag, Zr
8XXX	others	Fe, FeSi, FeSiCu

Table 4: Heat treatments of Al-Alloys [14]

Designation	Description
T1	Cooled from an elevated-temperature shaping process and naturally aged to a substantially stable condition
T2	Cooled from an elevated–temperature shaping process, cold worked, and naturally aged to a substantially stable condition
T3	Solution heat treated, cold worked, and naturally aged to a substantially stable condition
T4	Solution heat treated and naturally aged to a substantially stable condition
T5	Cooled from an elevated – temperature shaping process and artificially aged
T6	Solution heat treated and artificially aged
T7	Solution heat treated and overaged/stabilized
T8	Solution heat treated, cold worked, and artificially aged
T9	Solution heat treated, artificially aged, and cold worked
T10	Cooled from an elevated – temperature shaping process, cold worked and artificially aged.

Alloys, belonging to the series 2XXX, which have been investigated in the experimental section, are the subject of improvement/development within the COIN OPTIMATSTRUCT FFG project [4]. According to the Aluminum Association, the main alloying part besides aluminium is copper; whose alloys have favourable fatigue and high–temperature properties. Cu supports the strengthening by precipitation hardening, however at the same time it can increase the corrosion ability. Due to copper precipitates at the grain boundaries, pitting and stress corrosion becomes likely. Other alloying elements have differing influences on aluminium–copper alloys [18].

Typical applications for aluminium–copper alloys are the screw machine products, truck frames and wheels, aircraft structure, auto body panel sheet and for structures that are used at high temperature and for high–strength welding. [14]

The alloy 2618 is used for aircraft engines [14] and according to J.C Williams et.al. [19] it was also part of the primary structure of the Concorde. Applications of $AlCu_4Ti$ are automobiles, automotive engineering, engines, mechanical engineering, textile industry, and defence technology [20].

Zirconium and titanium shift the recrystallization temperature to higher temperatures, improving the welding behaviour and the fabrication ability. With increasing amounts of manganese and magnesium the tensile strength and yield strength goes up. With manganese, the ductility of the alloy can decrease, therefore not more than 1 wt% of it is usually added [18].

For aluminium-copper-magnesium alloys, the addition of nickel enhances the strength and hardness at higher temperatures; however, if the amount exceeds 0.5 wt%, a reduction of the tensile properties of heat-treated alloys at room temperature appears [18].

Addition of iron to aluminium–copper–nickel alloys leads to a higher strength at increased temperatures because of the fine grain size. Silver also increases the strength of aluminium–copper–magnesium alloys which are heat-treated and aged [18].

Addition of iron to aluminium–copper–nickel alloys leads to a higher strength at increased temperatures because of the fine grain size. Silver also increases the

strength of aluminium–copper–magnesium for alloys which are heat-treated and aged [18].

The high strength of aluminium–copper alloys originates from the precipitation of the supersaturated solid solution (SSSS). A typical general precipitation sequence for aluminium alloys is:

SSSS → Guinier – Preston zone 1 (GP[1]) → Guinier – Preston zone 2 (GP[2]) → metastable phases → stable phases

For aluminium–copper alloys the precipitation sequence is:

SSSS → GP[1] → GP[2] (Θ'') → Θ' → Θ (Al_2Cu)

The precipitation sequence for aluminium–copper–magnesium alloys is:

SSSS → GP[1] → GP[2] → S' → S (Al_2CuMg)

The occurrence of these phases depends on aging time and temperature. Figure 4 shows when the Guinier-Preston-Zones and the theta zones appear and how they look like. GP1 is a coherent copper–precipitate with a diameter between 5–10 nm and its thickness is one atomic layer. A fully coherent disc with around 20 nm diameters and a thickness of approximately 3 nm is the Guinier-Preston- zone 2. This zone is also known as Θ''-phase. The more of these precipitates exist, the higher the hardening effect. When the Θ'' phase grows further, the Θ' is formed. This phase is only partly coherent with the matrix. Both phases can exist in parallel at the highest strengthening level. The Θ-Phase (tetragonal Al_2Cu phases) occurs at over-aging and it is totally incoherent with the matrix [14, 21, 22].

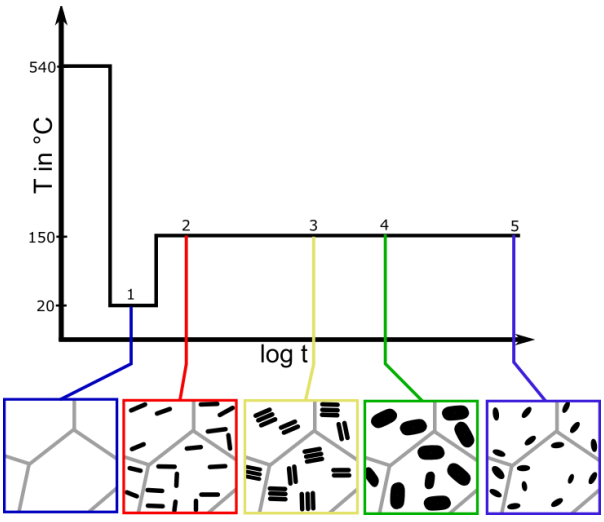

Figure 4: Sequence of precipitation structure at Al-Cu-alloys modified from University of Stuttgart [21]

3.2 Magnesium Alloys

In metallurgy magnesium can be applied in a wide range of different functions. Besides being used in magnesium-base alloys, Mg it is used as an alloying element, for cathodic protection in anodes and for desulfurizing steel. Applications are also in the field of organic chemistry where it is used as catalyst in Grignard reaction. [9]

Big advantages of magnesium alloys are the low density (approximately 1.8 kg/dm^3) and the favourable casting properties. These are part of the reasons, why magnesium is used for light products since more than 100 years. The first official alloy with magnesium as an addition was duralumin at the beginning of the 20th century. 90 years later (1990ies) magnesium based casting and wrought alloys make 20% of free-market magnesium shipments. Typical products where magnesium–alloys are used, are in the automobile and aircraft/aerospace industry, military industry, for electronics, sport utensils and everywhere where a weight reduction is requested [21, 23].

The nomenclature of magnesium–alloys follows the ASTM-standard (ASTM B275). Letters decode the main alloy elements and the numbers, describe the degree of alloying. Alloy AZ31 for instance contains aluminium (A) and zinc (Z) as the main alloying elements three weight percent of aluminium and one weight percent of zinc. Typical alloys with their abbreviations are listed in the table below. (Table 5) [14, 24]

A list of currently important magnesium-alloys is given in table 6. Typical alloying elements can be divided into two groups, actively influencing the melt. Beryllium and manganese belong to this group. They can reduce the rate of melt oxidation (beryllium) and the corrosion rate through the reduction of the iron content (manganese). These elements are added in very small amounts and their solubility in the melt is less important. Elements belonging to the second group are modifying the alloy's microstructure by means of hardening mechanisms such as solid solution hardening, work hardening, boundary hardening and particle dispersion hardening. They might also influence the castability of the alloys. Typical elements besides aluminium are copper, lithium, manganese, silver, yttrium, zinc and zirconium and some rare earth elements (cerium, lanthanum, neodymium, thorium). These elements need to have high solubility in liquid magnesium, and cause grain refinement. [14]

Table 5: Designation s for cast and wrought alloys [24]

Short letter	Alloy element	Frequency
A	Aluminium	Very often
B	Bismuth	Rare
C	Copper	Rare
D	Cadmium	Rare
E	Rare earth Elements	Often
F	Iron	Rare
H	Thorium	Rare
K	Zirconium	Often
L	Lithium	Rare
M	Manganese	Very often
N	Nickel	Rare
P	Lead	Rare
Q	Silver	Often
R	Chromium	Rare
S	Silicon	Often
T	Tin	Rare
W	Yttrium	Often
Y	Antimony	Rare
Z	Zinc	Very often

Table 6: Currently most magnesium alloy systems, with an emphasis on the creep resistant magnesium alloys [25]

Alloy systems	Examples	Alloying elements	Intermetallics
Mg–Al	AZ (31, 91) AM50, AE42, AS (41, 21) AX, AJ (51, 52, 62) ACM (522), MRI (153)	RE, Si, Ca, Sr,	Al_4RE, Al_2Si, Al_2Ca, $(Mg,Al)_2Ca$, Al–Ce, Mg–Al–Ca, Mg–Al–Sr
Mg–Zn	ZAX (8502, 8506, 8512), ZE, ZC	Al, Ca, RE, Cu	Mg–Al–Zn–Ca
Mg–RE **Mg–Ce** **Mg–Y** **Mg–Gd**	 MEZ WE (43, 54) Mg–Gd–Ye–Mn	 RE and Zn Nd Y and Mn	 $Mg_{12}RE$ $Mg_{14}Nd_2Y$, Mg_9Nd $Mg_5(Gd,Y)$, $Mg_3(Gd,Y)$
Mg–Sc	Mg–Sc–Mn, Mg–Sc–Ce–Mn	Mn, Ce	Mn_2Sc
Mg–Ag	QE (22)	RE (Nd)	$MgAl_{12}Nd$
Mg–Th	Mg–Th–Zr, Mg–Th–Zn–Zr	Zn and Zr	$Mg_{23}Th_6$
Mg–Sn	Mg–Sn–Ca, Mg–Sn–Al–Si (TAS831)	Ca, Al and Si	CaMgSn

A relatively new class of Mg alloys goes back to Shae K. Kim [20] and is called *Eco-magnesium* (Eco = Environment–conscious), which can be obtained when alkaline earth metal oxides (CaO, SrO), alkaline metal oxides (NaO, KO), or calcium compounds are added to the alloys. In industrial applications mostly calcium compounds such as CaO, $Ca(OH)_2$, $CaCN_2$ or also strontium oxides (SrO) are added, with CaO being in a range between 0.3–0.7 wt% for commercial wrought and cast alloys. 0.5 wt%-0.7 wt% of CaO is added to alloys with special purposes, like fire resistance or biodegradability. [20] The important advantages of Eco-magnesium are:

A) No need of SF6 environmental gases in the production process

B) Beryllium is eliminated

C) Improvement of the cleanness of the melt

D) Recyclability

E) Original process parameters adjustability for manufacturing processes and

F) Enhanced mechanical properties by grain refinement and inner consistence.

A typical microstructure (non-equilibrium solidification) of magnesium–aluminium–alloys without CaO has α–and β–phases. The α–phases are coarse dendrites and the β-phase is a bulk skeletal phase ($Mg_{17}Al_{12}$). By adding CaO, extra phases like Al_2Ca and $(Mg, Al)_2Ca$ are formed, leading to an altered microstructure and much finer grains, whereby Al_2Ca is enriched at the grain boundary [26].

During the OPTIMATSTRUCT project [4] different Eco-magnesium products have been produced and subsequently investigated by TEM. For this various sample preparation pathways have been tried out.

.

4. Methods

4.1 Transmission electron microscopy

Electron microscopy (EM) is a very important tool for material characterization, as it provides numerous possibilities of imaging and spectroscopic work down to the nano-scale. Depending on dimensions and type of information sought about the specimen, SEM (scanning electron microscope) or TEM (transmission electron microscope) techniques can be employed. [1, 3]

The basic principle of EM is the interaction of electrons (in vacuum) with the specimen and study of these interactions with appropriate detectors. As can be seen in Figure 5 different types of elastically or inelastically scattered electrons are generated upon interaction. Inelastic interaction leads to signals that can be used for different spectroscopic methods (EDX and EELS) as used in the TEM, which shall be the focus here. [1, 3]

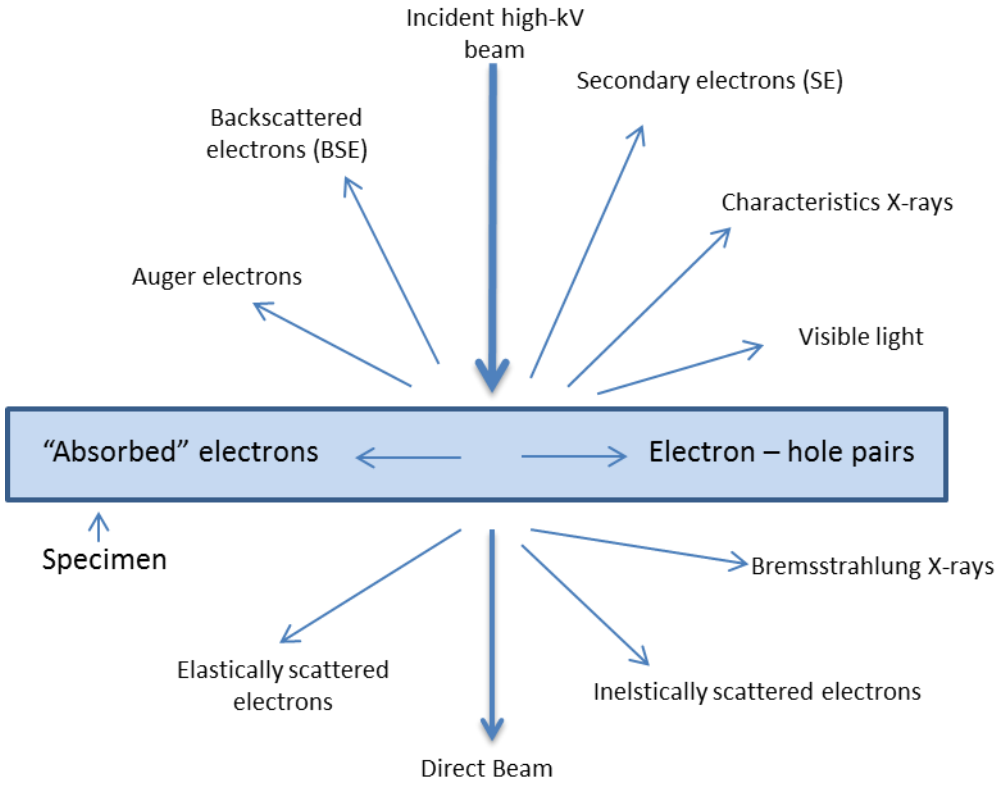

Figure 5: Electron-specimen interaction (modified from Wiliams and Carter 2009, figure 3.1) [3]

4.1.1 Setup and functioning of a transmission electron microscope

The basic setup of a transmission electron microscope (TEM) is shown in figure 6 and shall be described here. The first component is the emission section, consisting of an electron cathode and an acceleration anode. There are different types of electron guns, which can be categorized into thermionic sources and field-emission guns. Tungsten hairpin and LaB_6 (lanthanum hexaboride) filaments (thermionic) are single crystals heated up to a high temperature, however, upon emission, they are characterized by a low beam coherency. Field-emission guns can be separated into hot / Schottky-type or cold emission systems and are used for investigations, where highest spatial resolution and high quality spectra are needed. [1, 27, 28]

The lens system consists of electro–magnetic “zoom” lenses used for beam shaping and manipulation. Condenser lenses control the illumination of the sample by either a convergent or a parallel beam of electrons. The objective lens forms a first image of the sample and also a diffraction pattern at its back-focal plane. A set of projector lenses, after the objective lens, magnify the image or the diffraction pattern. An intermediate lens controls the information (image or diffraction pattern) that gets detected. Depending on the exact configuration of the microscope, additional lenses, lens aberration correctors, and other apertures (in addition to the condenser, objective and selected area aperture) can be added. [1, 27, 28]

The holder containing the sample is placed in the middle of the upper and lower pole pieces of the objective lens. Different requirements on the vacuum conditions at various stages of the microscope necessitate a complicated vacuum pumping system, consisting of turbo molecular and ion getter pumps. An airlock system is available at the goniometer, to control the insertion when coming from atmospheric pressure. [1, 27, 28]

Different illumination conditions define the type of microscope imaging mode. A broad parallel beam, which illuminates a large field of view, is used for bright–field, crystallographic dark–field, and high–resolution imaging. Also selected–area electron diffraction and chemical analysis (EDS, EELS) can be carried out in this mode. Nano diffraction, convergent beam electron diffraction and annular dark–field imaging and all sorts of nano-analytical investigations require a convergent electron beam. [1, 27, 28]

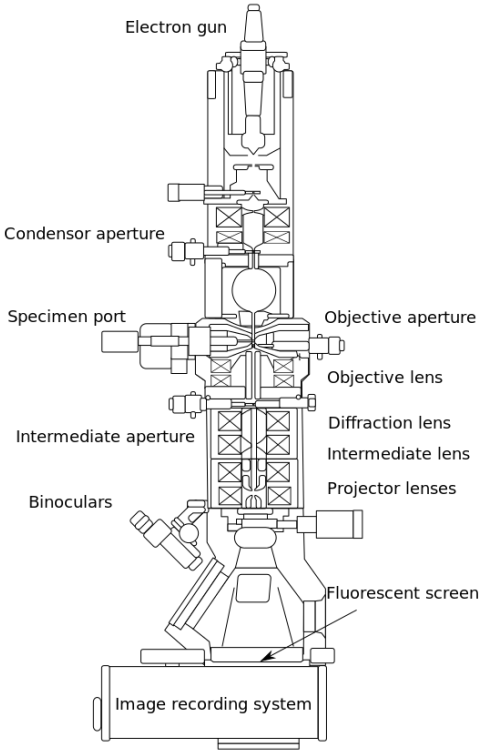

Figure 6: General construction of a transmission electron microscope [29]

4.1.2 Operating modes

Bright–field /Dark–field mode

Often the TEM is operated in bright-field mode. By selecting the direct, undiffracted beam, a bright-field image is obtained, whereas if one of the diffraction spots from the electron diffraction pattern is selected, a dark-field image can be formed. Both, bright–field and dark–field images, rely on different forms of amplitude contrast (mass-thickness or diffraction contrast). An inserted objective aperture performs this angular choice of electrons for imaging. [1, 3, 27]

High–resolution TEM (HRTEM)

High–resolution imaging relies on pure phase changes of the beam when traversing the sample (has to be crystalline) and occurs when at least two beams (undiffracted and diffracted) interfere with each other. As a result lattice fringes can be observed which are related to the local atomic arrangement (crystal structure) and orientation. [1, 3]

Scanning TEM (STEM)

In contrast to the conventional TEM imaging, a small probe can scan the specimen pixel per pixel in STEM mode. This is achieved by sufficient demagnification of the source by the condenser lenses and the objective lens, acting as an additional condenser lens. The image can be acquired by detecting different angles of scatter with dedicated bright–field, dark–field or high angle annular dark–field STEM detectors. [3, 27]

Energy dispersive x–ray spectroscopy (EDXS)

This type of spectroscopy is based on the emitted x–rays of the atoms, which are characteristic for each element. Due to primary electrons, atoms are ionized at an inner shell. By filling the inner hole with an electron from an upper shell, excess energy is set free in the form of x–rays. This method is more sensitive to atoms for higher atomic numbers. Typical detectors are lithium drifted silicon detectors or high-purity intrinsic germanium detectors. The basic detection principle bases on the resulting electron-hole pair in the material due to the incoming x-rays. Each characteristic energy quantum is proportional to the resulted charge carriers. [1, 27]

Electron energy loss spectroscopy (EELS)

EELS analyses energy losses of the inelastically scattered electrons. The amount of the energy lost can be characteristic for each element, when looking at inner-shell ionization edges. This method is more effective for low atomic numbers than for high atomic numbers. By using this method, qualitative and quantitative analysis regarding elemental composition, can be carried out and measurements of (the relative)

specimen thickness, is possible. After the beam transmitted through the sample, it passes an entrance aperture and is focused with an electron lens. A magnetic prism with a drift tube spread the beam into the different energy containing electrons. After a multipole optic the beam encounters a detector which can be a CCD or a photodiode. [1, 3]

Energy filtered TEM (EFTEM)

EFTEM is an imaging mode based on EELS. Images with particular energy loss information can be acquired by using a defined energy window, which can be positioned anywhere in the spectrum but for elemental mapping has to be placed at an edge. The energy filter can be inside the microscope column (in–column system) or after the column (post–column system) [30]. Possible other applications are contrast enhancement and zero-loss filtered diffraction, thickness mapping, and chemical bond mapping, by making use of the edge fine-structures. The selected energies are ionization energies for each element or the zero–loss energy. [3]

Thickness determination (t/λ)

A typical method for assessing a specimen thickness is the Log-Ratio method. This method measures the thickness by comparing a zero–loss image or spectrum (I_0 = area under the zero-loss peak) and a normal unfiltered bright–field image (I = area under the whole spectrum). The used equation: $t/\lambda = \ln (I/I_0)$ bases on the Poisson statistic. λ is the total mean free path for all inelastic scattering events in a specific material. According to R.F. Egerton [31] a typical λ value for pure aluminium is at 200keV 134 nm.

With this method relative thickness maps are calculated. The aim at the experimental part is to have thin areas which are lower than 1, and ideal for high resolution investigations would be a thickness of 0.4.

4.2 Instruments

4.2.1 Preparation devices:

TenuPol–5 ®

The main preparation device, which was used for the preparation, was the TenuPol-5 from Struers. Usually it is used for automatically electrolyte polishing. The principle is part of the chemical and electropolishing methods as mentioned in chapter 2.2.1. The specimen is polished from both sides. The process stops, when a hole occurs and the infrared light pass through the hole in the sample. [32]

PIPS (Precision Ion Polishing System) ®

This device (as build and commercially distributed by Gatan) was used for post treatment after electropolishing or as a final thinning method. The principle is based on the ion milling, which is explained in chapter 2.2.2. It has miniature Penning ion guns with set angels to 4° from above and 6° from down relative to the specimen and the energy of the guns is typically between 2–4 keV. The thinning happens alternately from both sides and an optical stereo microscope is installed to monitor the process. [32]

FIB/SEM Dual Beam Microscope FEI NOVA200 ®

The FIB (focused ion beam by FEI Company) was used, for the preparation of site-specific TEM lamellas, with a thickness of less than 50 nm (chapter 5.3.8). In this case gallium ions are directed towards the sample and scanned over the surface to remove material. [32]

NANOMILL ®

This device is used for post treatments, mainly after FIB preparations (chapter 5.3.8). The principle is a low energy milling, with an argon ion beam, to remove the upper layers of the specimen. Usually the energy of the beam can be varied between 50 eV–2 kV, and as a monitoring system a secondary electron detector (Everhardt-

Thornley principle) is used. The following parameters can be varied to obtain the best result: milling angles, specimen position, temperature down to -175°C and the processing time. [33]

Plasma Cleaner

Another possibility for a post treatment is the Plasma Cleaner. The aim of the plasma cleaner is to remove possible contaminations and amorphous layers form the specimen and the holder with the plasma. By an oscillating electromagnetic field, free electrons are accelerated to a high velocity and due to collisions gas atoms are excite and plasma is induced. Plasma ions impinged the sample surface with low energies depending on the set conditions (input power, chamber configuration and pressure, and electrode configuration). Typical gas mixtures are 25% oxygen and 75% argon and also 80% Helium and 20% argon. [34,35]

Leica Ultra UCT with Leica EM FCS

This microtome by Leica was used for cutting semi– and ultrathin sections of Magnesium and its alloys. With an extra add-on like a special cooling chamber (Leica Ultra UTC), cryo microtomy was possible. This method is explained in more detail in chapter 2.2.3. [32]

4.2.2 Microscope devices

4.2.2.1 OM

Zeiss Axioplan with Axio Cam ICc1

This optical microscope was used in order to control the surface and the holes of the specimen. [32]

4.2.2.2 TEMs

Philips CM 20

The electron source of this microscope is a LaB_6 – cathode and it works with an accelerating voltage of 200 kV. For EFTEM imaging a Gatan 678 imaging filter (GIF) is installed. This provides the acquisition of energy filtered images with a lateral resolution down to about 1 nm. This microscope was used in order to check the thickness of the specimens. [32]

FEI Tecnai 12

This microscope works with an accelerating voltage of 120 kV and it has a LaB6 as an electron source. The magnification range is between 35x to 700000x. This microscope is used mostly for biological and for cryo–samples, since the cryo transfer holder suits. It was used to check the cryo–microtome cut sample. [32]

FEI Tecnai F20

The Tecnai F20 works with a monochromated FEG (Schottky Field Emitter) at a maximum accelerating voltage of 200 kV. The microscope is equipped with a Gatan GIF Quantum with Dual EELS and High–Speed Spectrum imaging, an EDAX Saphire Si(Li) detector for x–ray analysis and a Gatan UltraScan CCD. The TEM magnification ranges from 25x to 2000000x. The STEM magnification is between 100x and 5Mx and it has a Digiscan II with BF, ADF and HAADF cameras. This microscope was used for energy–filtered imaging (elemental maps, t/λ), high–resolution TEM and EELS/EDX in STEM mode. [32]

FEI TITAN^3 G2 60–300 – Austrian Scanning Transmission Electron Microscope (ASTEM)

This microscope is a probe–corrected high end TEM/STEM system. It is equipped with a high brightness electron gun (FEI X–FEG) and a monochromator for enhancing the energy resolution (0.25 eV). The acceleration voltage ranges from 60 to 300 kV. For high resolution STEM imaging (< 70 pm) a Cs probe corrector (DCOR) is installed. For imaging and analytical investigations a high–sensitive energy

dispersive X–ray spectrometer (FEI ChemiSTEM technology with Super–X detector by Bruker), a high–end post–column electron energy filter with “Dual EELS” capability and a fast electrostatic shutter by Gatan Inc (GIF Quantum ERS^{TM}) is mounted.

It was used for energy–filtered imaging (elemental maps, t/λ), high–resolution TEM, high–resolution STEM imaging and EELS/EDX spectrum imaging. [32]

5. Experimental

5.1 Basic preparation procedure

The aluminium- and magnesium-alloys run through the same pre–preparation steps. The AA2618 T6 and $AlCu_4Ti_{0.2}$ T6 bulk were cut with a handsaw into smaller pieces, which are suitable for cutting fine slices. The other alloys were already in the appropriate size. Thin slices with a thickness of around 500 µm are cut off with a diamond wire saw from Well or with a blade saw (IsoMet® 1000 Precision saw) from BUEHLER. From these thin slices, discs with a diameter of 3 mm were blanked out with a disc punch (Gatan). A disc grinder 623 (Gatan) with abrasive paper (CarbiMet Grit 320/400/600; BUEHLER) was used to reduce the thickness to approximately 150 µm. The thickness was measured with a thickness gauge of DR. JOHANNES HEIDEHAIN.

These specimens can be used for different final preparations. The main focus was on electropolishing which, however was partially followed by a post treatment with PIPS for smoothing and improving the surface.

Other final preparations were tried with PIPS (Precision Ion Polishing System, Gatan), FIB/SEM (Focused Ion beam, FEI), NANOMILL (Fischione) and by cryo–microtomy for the magnesium alloy.

The final thinning by electropolishing with TenuPol-5 has to be done at lower temperatures; therefore the electrolyte had to be cooled down. By using the freezer a temperature of around -10°C was reached. For even lower temperatures (-20°C and -40°C) the trough with the electrolyte was cooled with carbon dioxide snow which is further mentioned as dry ice. Right after the electropolishing the specimens were washed in Ethanol or Methanol, which is mostly the constituent of the used electrolyte.

For the post treatment the specimens were inserted into the PIPS for a few minutes at a specific electron voltage and under specific beams angle.

5.2 Preparation and investigation of aluminium-alloys

The electro-chemical preparation was done with the TenuPol-5. The following table presents a list of the electrolytes used to prepare the different aluminium alloys. For comparison, one specimen was prepared only with PIPS.

Table 7: List of the electrolytes and prepared aluminium alloys

Electrolyte	Composition	Alloys
1 [36]	90 ml dist. Water 730 ml Methanol 100 ml 2-butoxy-ethanol 78 ml Perchloric acid	AA2016
2 [37]	330 ml HNO_3 670 ml Methanol	AA2618
3 [38]	100 ml HNO_3 900 ml Methanol	AA2618 T6, AA2016, $AlCu_4Ti_{0.2}$ T6
4 [39]	50 ml Perchloric acid 950 ml Methanol	AA2618

The detailed preparations of the different alloys are explained in the next sub-chapters.

5.2.1 AA2016

Preparation with Electrolyte 1

The first electrolyte was indicated by the Struers Company for aluminium alloys. The pre-set values at the device were: a flowrate of 13, 5°C temperature and a voltage of 40 V. The flowrate describes the rate at which the electrolyte impinged the specimen.

The first test series was done by varying the voltage from 30 V to 50 V with steps of 5 V. For verifying also test series from 5 V–20 V, 15 V–35 V and 45 V–60 V each with steps of 5 V were done. The temperature for the preparation series varied between -4°C and -15°C. Before the preparation, the electrolyte was cooled down in

the freezer. After the electro polishing the specimen were washed in two glass dishes with Ethanol.

The detailed preparation parameters are given in the appendix (aluminium preparation experiment 1–4).

The first sample (a156) investigated by TEM was the one prepared with 30 V from the first testing series (Exp. 1). In figure 7 a bright field zero loss (ZL) filtered TEM image, and a HR TEM image and in figure 8 a relative thickness map with the corresponding ZL and bright field images are shown. The sample is thin but good high resolution imaging was not possible, due to an existent amorphous layer.

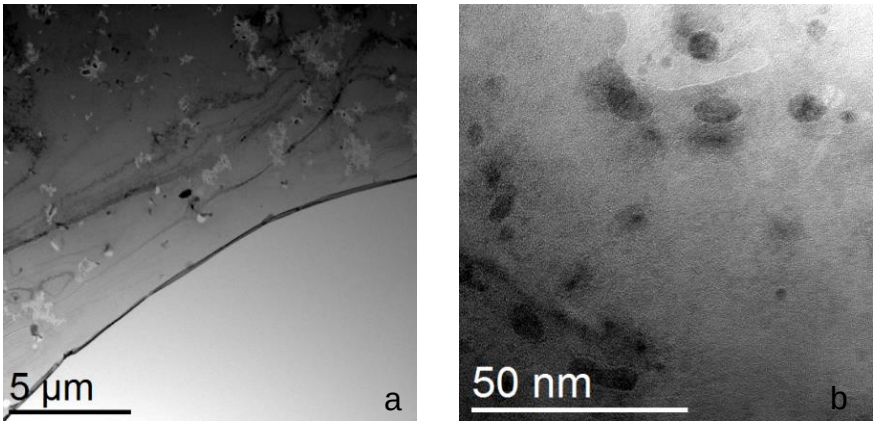

Figure 7: AA2016, prepared with electrolyte 1, 30 V (a) ZL TEM and (b) HRTEM (TF20, 200 kV)

Even the surface appears flat; at higher magnification it is uneven and also a little bit affected. Uneven surfaces are difficult to focus at higher magnifications; therefore high resolution images are practically feasible. Affected surface means that the sample was more etched than polished; due to the usage of incorrect preparation parameters a material selective removal occurred. Moreover caused by atmospheric oxygen the formation of a native oxide layer was inevitable.

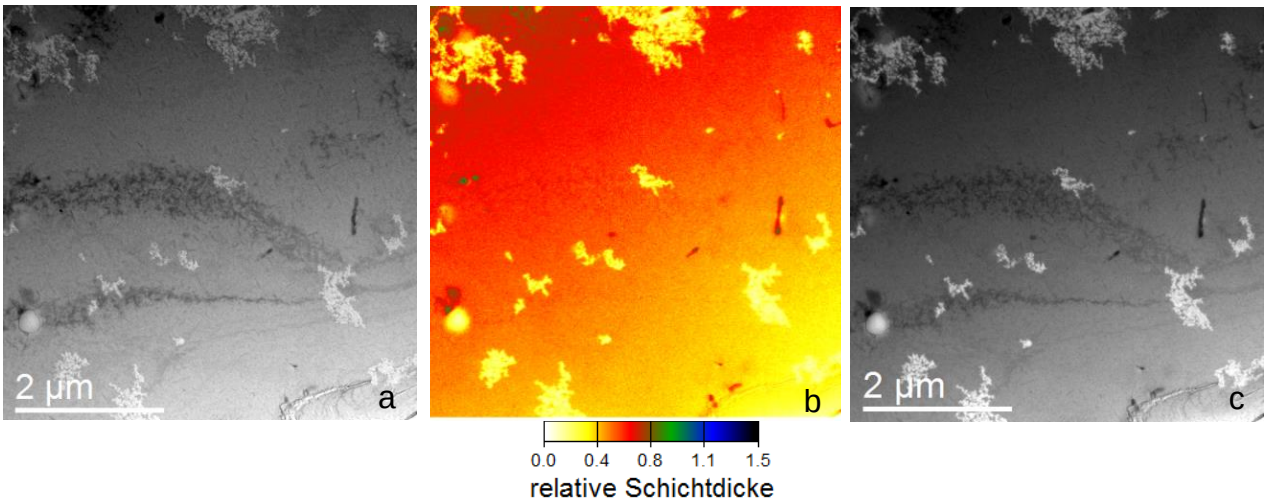

Figure 8: AA2016, prepared with electrolyte 1, 30 V, (a) BF TEM, (b) thickness map t/λ and (c) ZL BF image (TF20, 200 kV)

Consequently the samples were inserted in the PIPS for a short post treatment (4 min 30 s). Figure 9 and 10 show OM images before and after the PIPS of the sample which was prepared with 35 V (b155, Exp. 1).

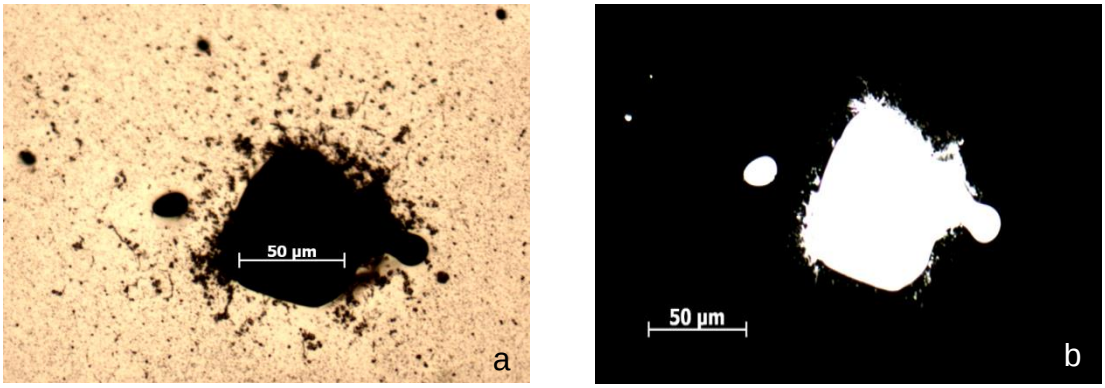

Figure 9: AA2016 prepared with electrolyte 1, 35 V, (a) reflected light image and, (b) transmitted light image (OM)

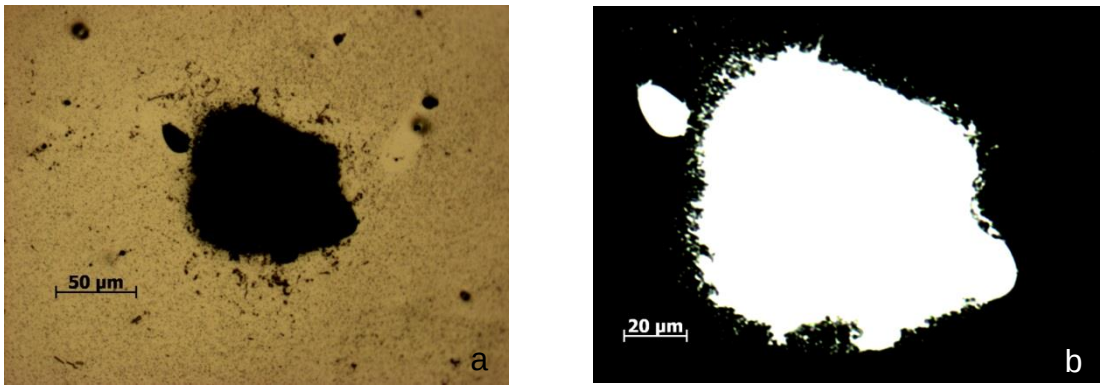

Figure 10: AA2016 prepared with electrolyte 1, 35 V after 4 min 30s in PIPS (a) reflected light image and, (b) transmitted light image (OM)

The size and edge of the holes changed; also the surface is homogeneously smooth. The sample was further investigated at TF20 at 200 kV. Figure 11 shows images with high resolution, indicated that the post treatment with PIPS was successful.

Figure 12 also shows the comparison of the voltage with the resulting hole size. The biggest hole was at 40 V, which however was the pre-set voltage at the device. Nevertheless this graph cannot display how the edges of the hole look like and whether an adequate sample quality is reached.

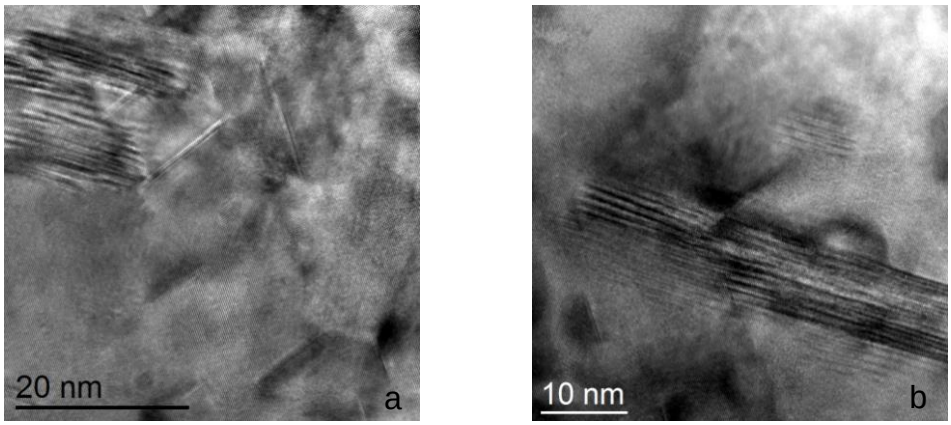

Figure 11: AA2016, prepared with electrolyte 1, 35 V + 4min 30s PIPS (a) HR ZL TEM Background filtered image and (b) HR ZL TEM (TF20 200 kV)

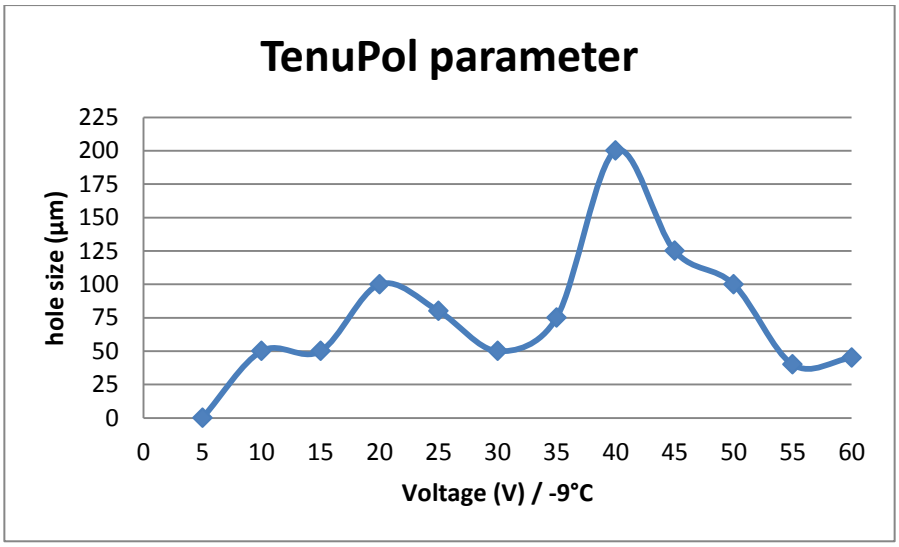

Figure 12: Graph which compares the resulting hole size with the used preparation voltage, AA2016, electrolyte 1

Due to the investigations at TF20, OM and visual inspection at CM20 (the GIF was not working because of technical problems), the samples which were prepared with 20 V and 35 V were decided to be favourable on the basis of the good results of exp. 1 b155 and exp. 2 d155. With those voltages, testing series with a change of the flowrate from 10 to 20 with steps of two were done (Aluminium experiment 5 and 6). With both voltages a graph was drawn, which compares the size of the hole with the flowrate (figure 13). The biggest hole size was in both cases with flowrate 14. Because the value is so close to on the TenuPol-5 pre-set flowrate 13, flowrate 13 was chosen for the subsequent experiments.

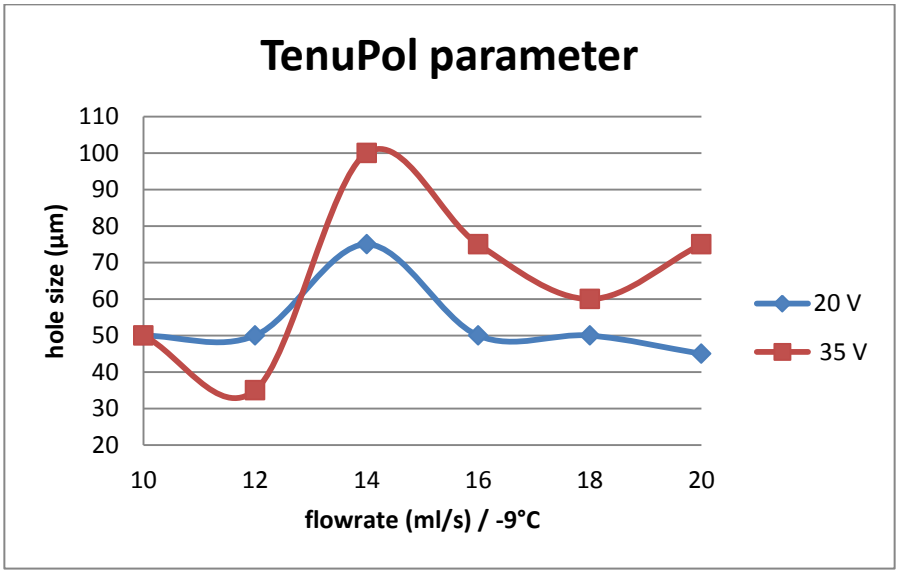

Figure 13: Graph which compares the resulting hole size with the used preparation flowrate with 20 V and 35 V, AA2016, electrolyte 1

The results of the flowrate testing series at 20 V were not as good as expected. The sample with a flowrate of 10 (Exp.5, a145) was thin, but the surface was uneven. The surface structure was visible but still attacked (figure 14 (a)). Hence it was inserted into the PIPS for two minutes, but all thin areas disappeared. The sample with a flowrate of 12 (Exp. 5, b156) was too thick after electropolishing and got also a post treatment with PIPS. Although the surface was flat, it was still thick. The next sample (flowrate 14, Exp. 5, c157) had no electron transparent areas; the post treatment would take too long to get thin areas. Also the sample with the flowrate 18 (Exp. 5, e144) did not change after the post treatment and was still not investigable. The best samples were those with a flowrate of 16 (Exp. 5, d161) and 20 (Exp. 5, 164) and a post treatment with the PIPS. Figure 14 (a) shows the surface of sample a145 (FR 10) without a post treatment and (b) shows the large thin areas of the sample prepared with the flowrate 16 and a PIPS treatment (d161).

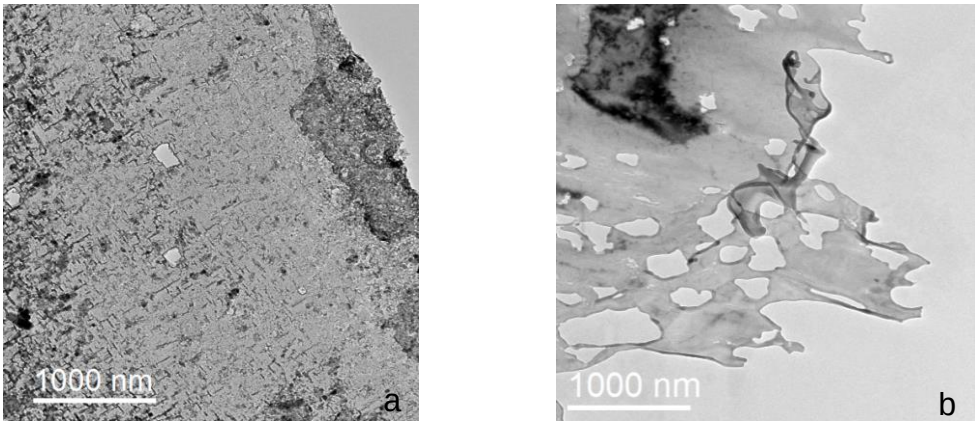

Figure 14: AA2016, electrolyte 1, 20 V (CM20, 200 kV) (a) BF with flowrate 10 and (b) BF with flowrate 16 + PIPS post treatment

The flowrate testing series at 35 V (Appendix: Aluminium Exp. 6) shows the following results. The sample with a flowrate of 10 (Exp. 6, a148) had, after PIPS treatment, a thin and even surface. In the investigation with TF20 at 200 kV, the sample showed a too thick oxidation layer; therefore high resolution investigations were not possible. The thin areas of the other samples (flowrate 14, 18 and 20 [Exp. 6, c143, e148, f149]) looked etched and not polished with small holes what indicate a selective etching process. This problem is visible in figure 15.

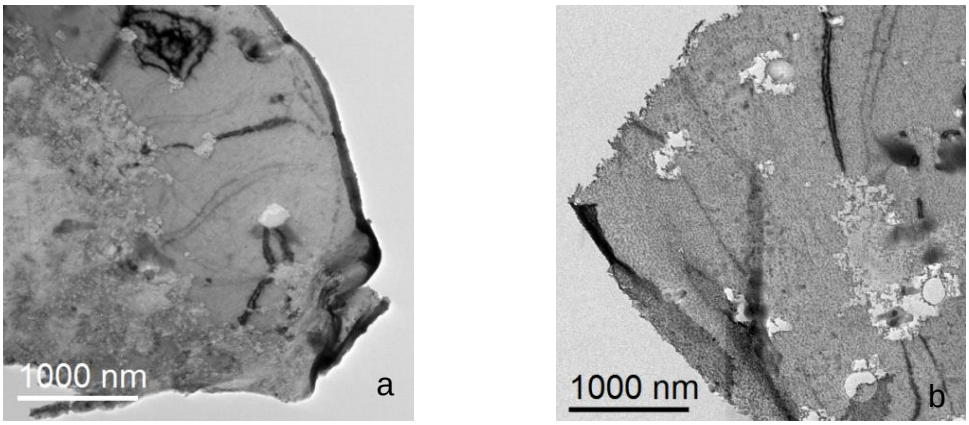

Figure 15: AA2016, electrolyte 1, 35 V (CM20, at 200 kV) (a) BF at FR 14 and (b) BF FR 18

Comparing the experiments which were done, we can conclude that the best result was at 35 V with a flowrate of 13 and a PIPS post treatment. These parameters were checked for reproducibility, first with a temperature of -6°C and then with a temperature of -20°C. The best results were achieved at -20°C plus PIPS post treatment. In figure 16 a BF image (a), a zero-loss BF image (c) and its relative

thickness image t/λ (b) are shown. The images show a really thin wide area. Also the high resolution image and its FFT image (Fourier transformed images, show the lattice structure of the material) show that the amorphous layer is very thin, (the spots are clearly visible without a huge amount of diffuse background around them (figure 17).

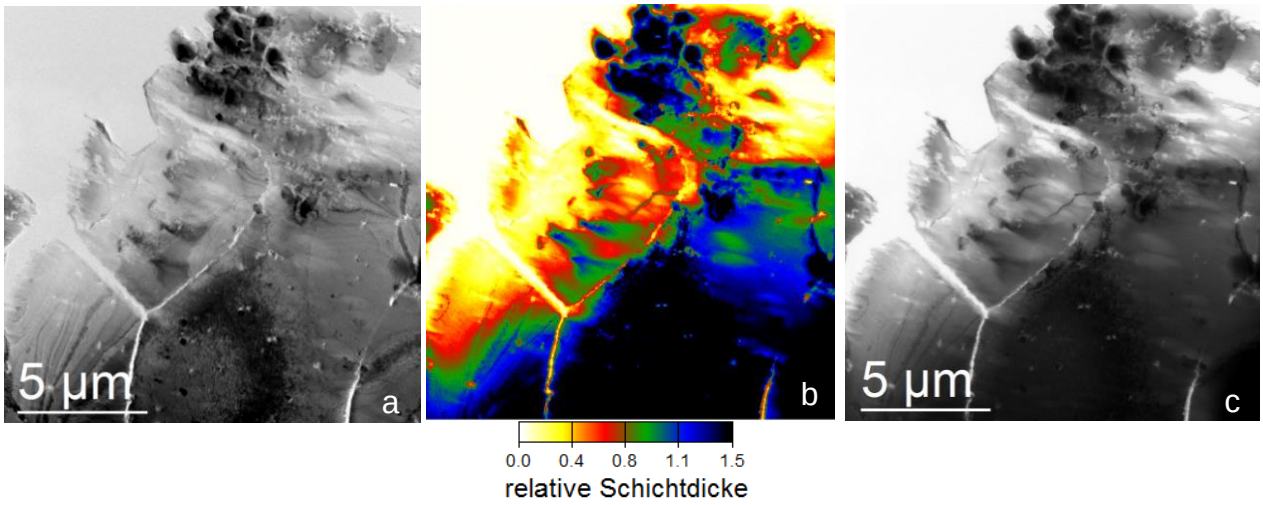

Figure 17: AA2016, electrolyte 1, 35 V, FR 13, -20°C, PIPS treatment (TITAN, 300 kV) (a) BF, (b) t/λ thickness image and (c) ZL BF

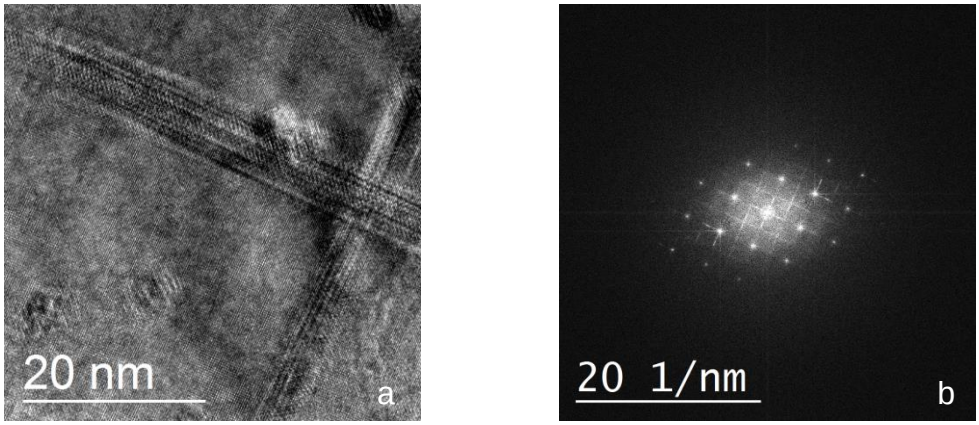

Figure 16: AA2016, electrolyte 1, 35 V, FR 13, -20°C, PIPS treatment (TITAN, 300 kV, TEM Mode), (a) HR TEM image and (b) the FFT of (a)

The preparation with the ideal parameters (35 V, flowrate 13, electrolyte temperature -20°C and PIPS post treatment) was tried again with 4 samples (A-D) of the same alloy (see appendix: aluminium, experiment 9). The difference of the samples is that each of them got a treatment after they were produced (e.g. heat treatment). Images of sample A (Exp. 9, Sample A, b150) are seen in Figure 18. The preparation shows thin areas (Figure 18 (a)), but the amorphous layer seems too thick for good high–resolution.

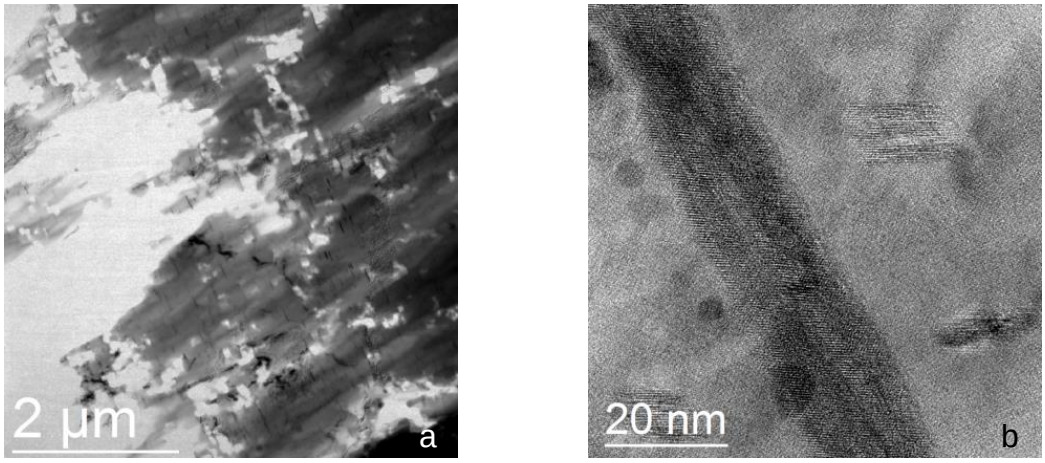

Figure 18: AA2016, sample A, electrolyte 1, 35 V, FR 13, -20°C, PIPS treatment (TITAN 300 kV) (a) BF TEM, and (b) HR TEM

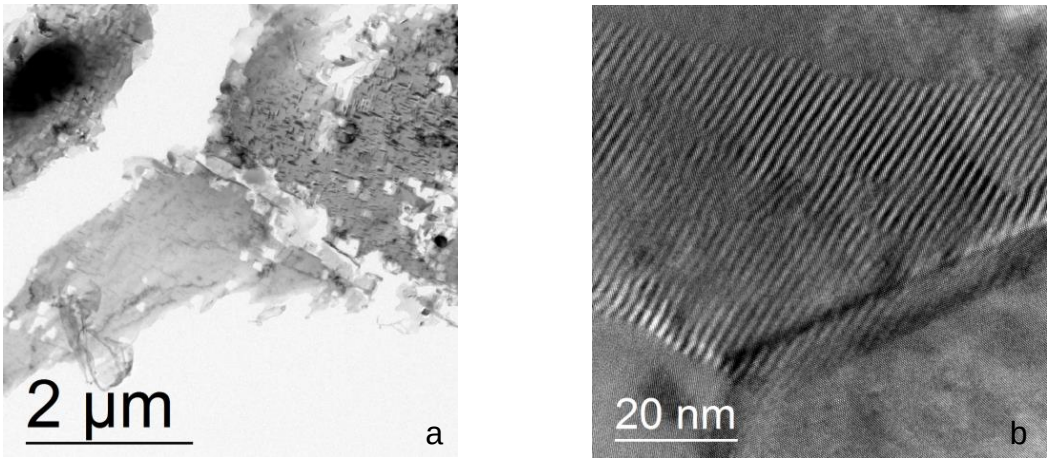

Figure 19: AA2016, sample B, electrolyte 1, 35 V, FR 13, -20°C, PIPS treatment (TITAN 300 kV)

Figure 19a shows an overview and 19b a high resolution image of sample B (Exp. 9, Sample B, b154). In the high resolution image a Moiré pattern can be seen, which indicates that the preparation worked better and high imaging was possible.

An image of the prepared sample C (Exp. 9, Sample C, b149) is visible in figure 20. In the image an overview and a particle at a higher resolution is visible. The surface

of the particle looks not clear, for that reason a short additional PIPS treatment were done. The surface appears clearer and the structure is better visible, also at a higher magnification (Figure 21).

Sample D (Exp. 9, Sample D, b162) had wide and electron transparent areas, but for good high resolution imaging the oxidation layer has to be reduced (Figure 22)

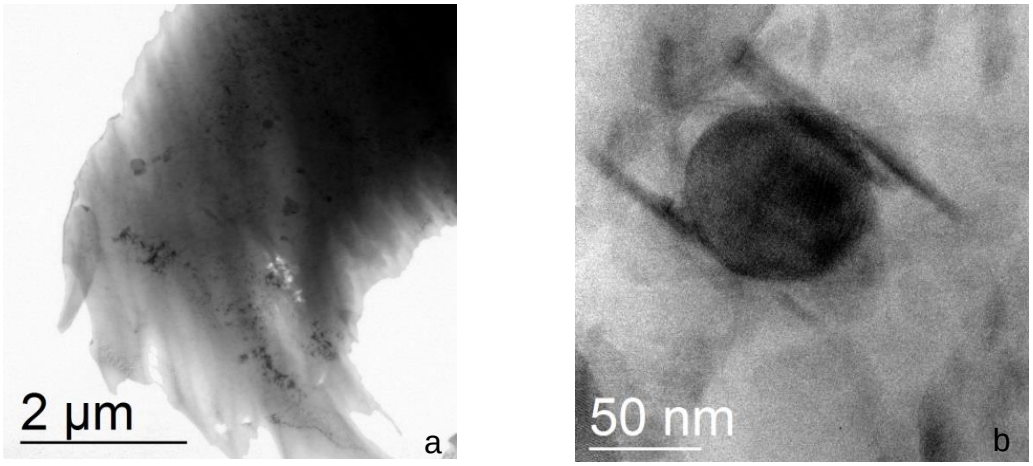

Figure 20: AA2016, sample C, electrolyte 1, 35 V, FR 13, -20°C, PIPS treatment (TITAN 300 kV, TEM image)

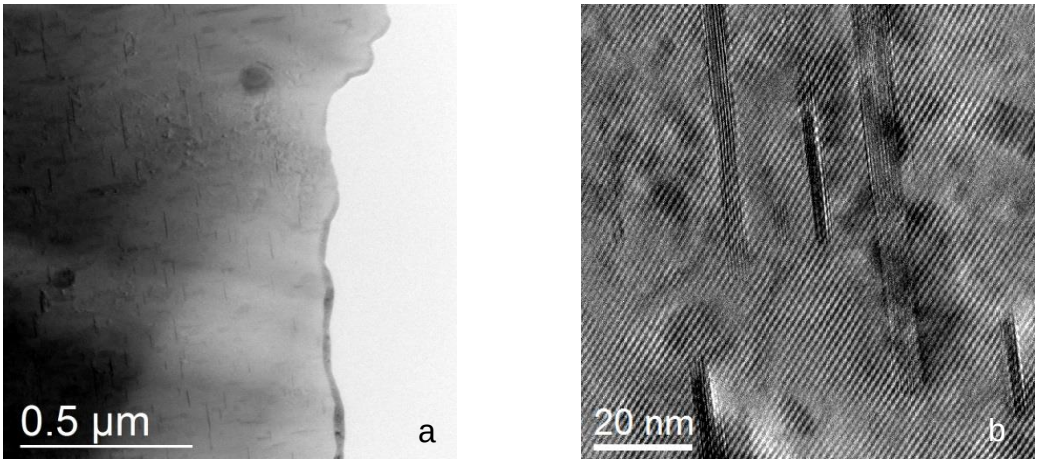

Figure 21: AA2016, sample C, electrolyte 1, 35 V, FR 13, -20°C + 2 x PIPS treatment (TITAN, 300 kV, TEM image)

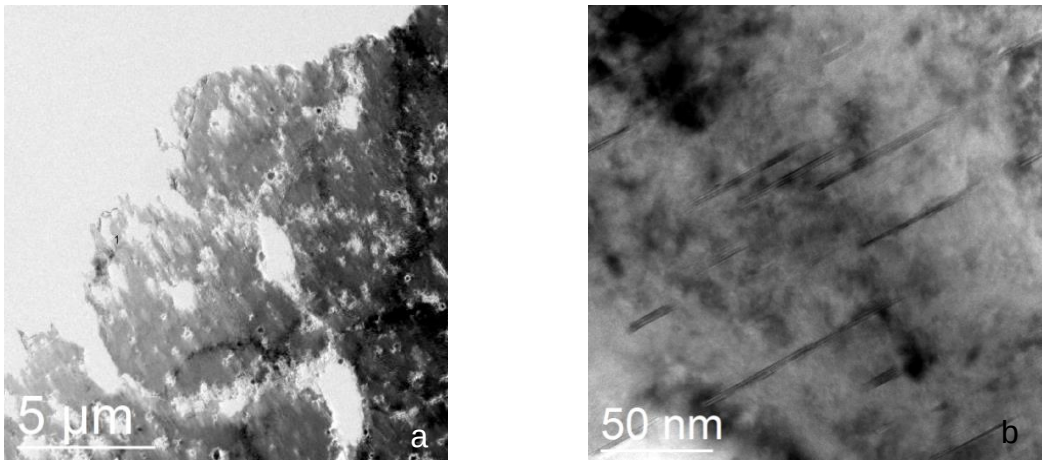

Figure 22: AA2016, sample D, electrolyte 1, 35 V, FR 13, -20°C, PIPS treatment (TITAN, 300 kV, TEM images)

Preparation with Electrolyte 3

Electrolyte 3 was used for AA2016 as well, because the first preparation with this electrolyte of alloy AA2618 (see 5.2.2) implicated a good preparation result.

The following parameters were tested: flowrate 13, electrolyte temperature -20°C and the voltage was varied between 10 V and 35 V by steps of 5 V. The detailed preparation is given in the appendix (aluminium preparation, experiment 12). After the preparation the samples were investigated with the OM. The surface has a structured appearance (figure 23 a, Exp. 12, c145), induced of the evolved wrinkles on the surface. These wrinkles occurred during the electropolishing at voltages between 10 V and 20 V. At voltages higher than 20 V the surfaces seems to be smoothed, see figure 23 b (Exp. 12, d164). However the edges of the prepared samples at higher voltages were less electron transparent (Figure 24, Exp.12, d164).

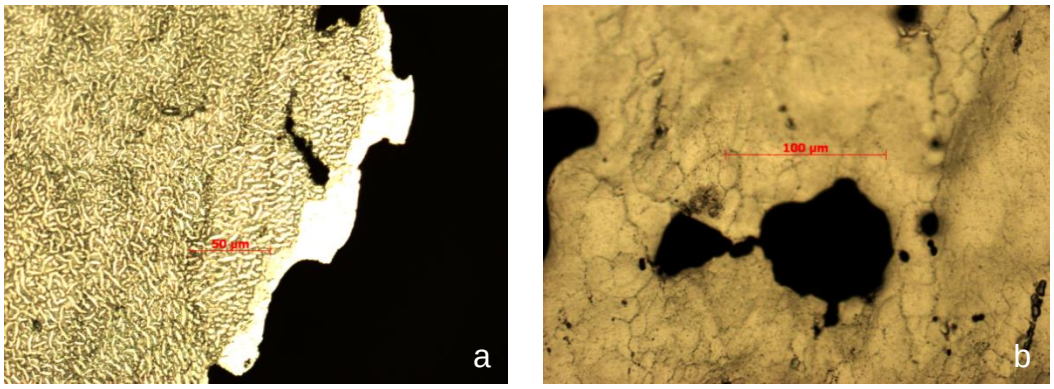

Figure 23:AA2016, prepared with electrolyte 3, (a) 20 V and (b) 25 V, reflected light image

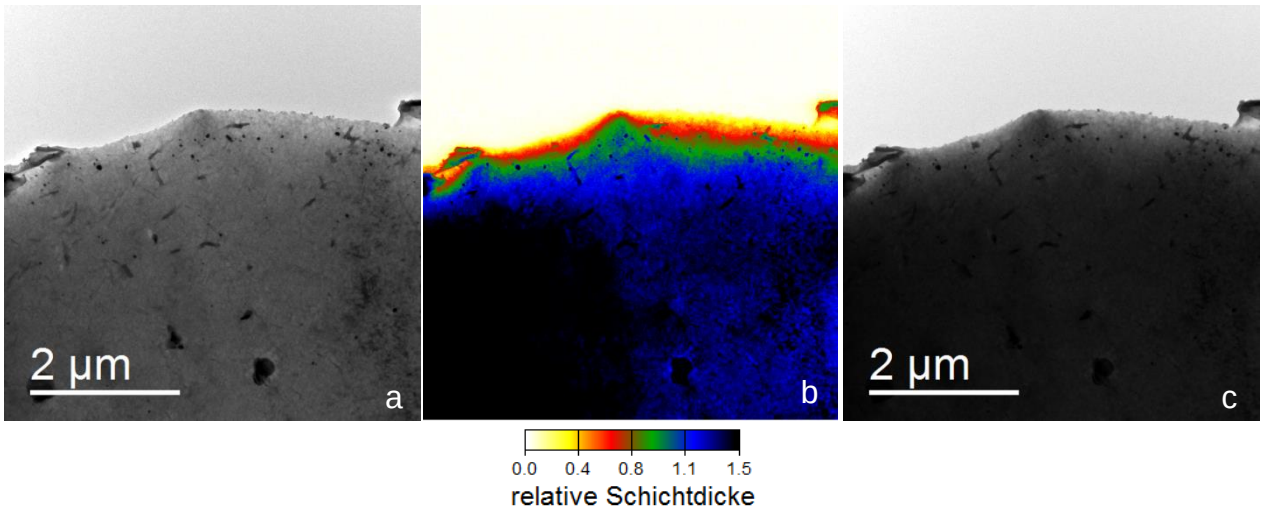

Figure 24: AA2016, prepared with electrolyte 3, 25 V (a) BF, (b) t/λ and (c) ZL BF image (TF20, 200 kV)

As a result electrolyte 3 is recommendable but further preparations and investigations after an additional PIPS treatment were necessary.

5.2.2 AA2618 T6

Preparation with Electrolyte 2

This alloy was prepared by using the electrolyte from Teichmann [38]. For the preparation, the temperature was set to -20°C, the flowrate to 13 and the voltage was varied between 10 V to 35 V with steps of 5 V (Appendix: Aluminium experiment 10).

The prepared TEM samples have already smooth surfaces in OM. All samples from this voltage variation series were investigated by TEM in CM20 (200 kV). The samples which were prepared with voltages of 10 V (Exp. 10, a166), 25 V (Exp. 10, d165) and 30 V (Exp. 10, e169) were not useful; the areas around the holes were not electron transparent. Also the sample with 15 V (Exp. 10, b168) was thicker, but the surface seemed evenly (Figure 25 (a)). The best samples were obtained for 20 V (Exp.10, c160) and 35 V (Exp.10, f167). Thin areas and a flat surface were present; the microstructure of the material was visible as well (25 (b-f)).

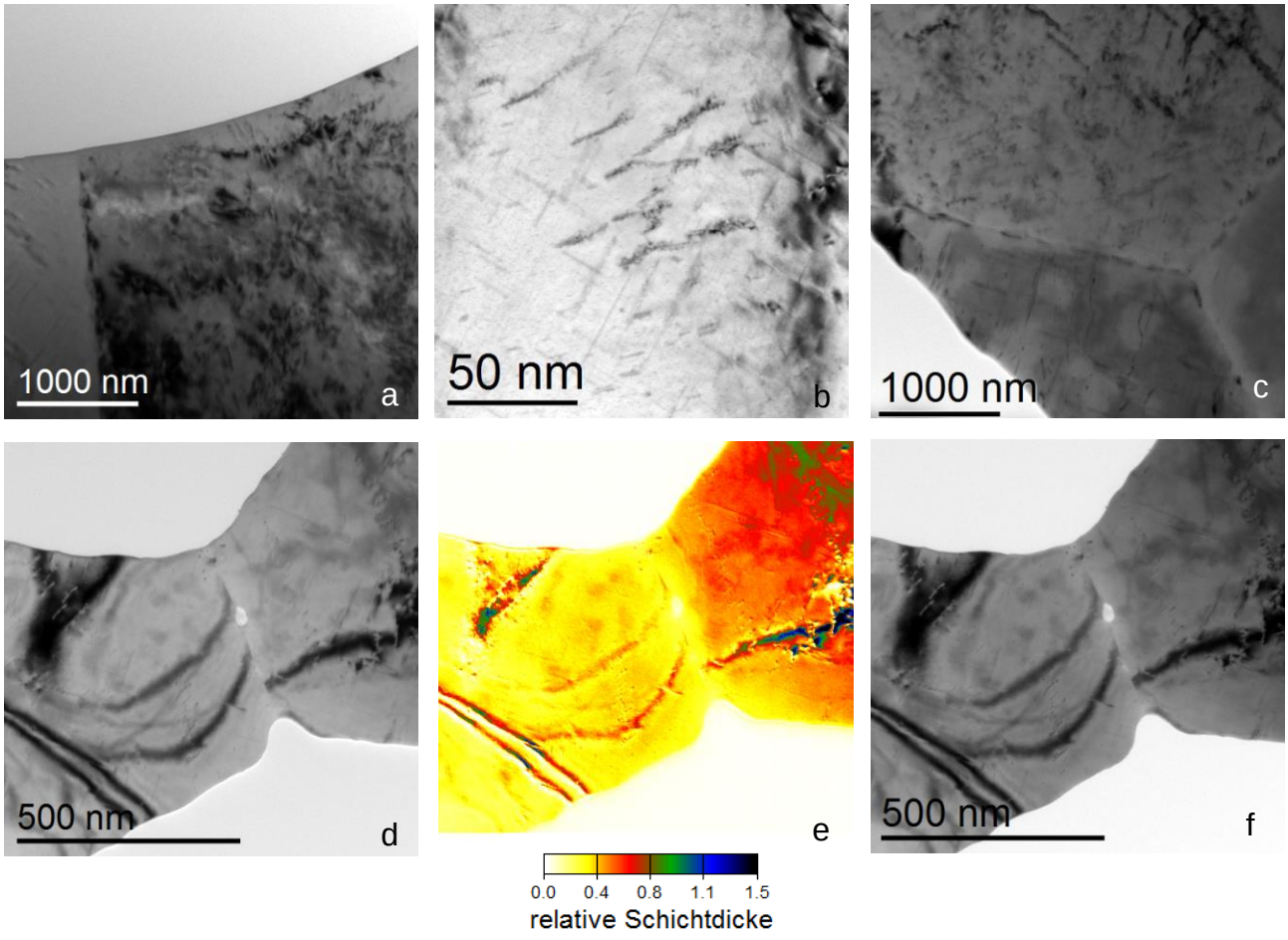

Figure 25: AA2618 T6 prepared with Electrolyte 2, (CM20, 200 kV) (a) BF TEM (15 V), (b) ZL BF TEM (20 V), (c) BF TEM (35 V), (d) BF TEM (35 V), (e) thickness map t/λ (35 V) and (f) ZL BF TEM (35 V)

The sample which was prepared at 20 V (Exp. 10, c160) was investigated in TITAN at 60 kV. Before the investigation a post treatment with PIPS for 1 min 15 s at 4 keV was necessary, due to the fact that the time gap between CM20 and TITAN investigation was too long. After the PIPS treatment the oxidation layer was reduced, thus that high resolution imaging was successful and small precipitates could be observed (Figure 26). Figure 27 illustrate a high resolution image, with the red marked area analysed with STEM EDX spectrum image. The particle shows a core–shell structure, with a core of silicon and magnesium atoms and a shell of copper atoms.

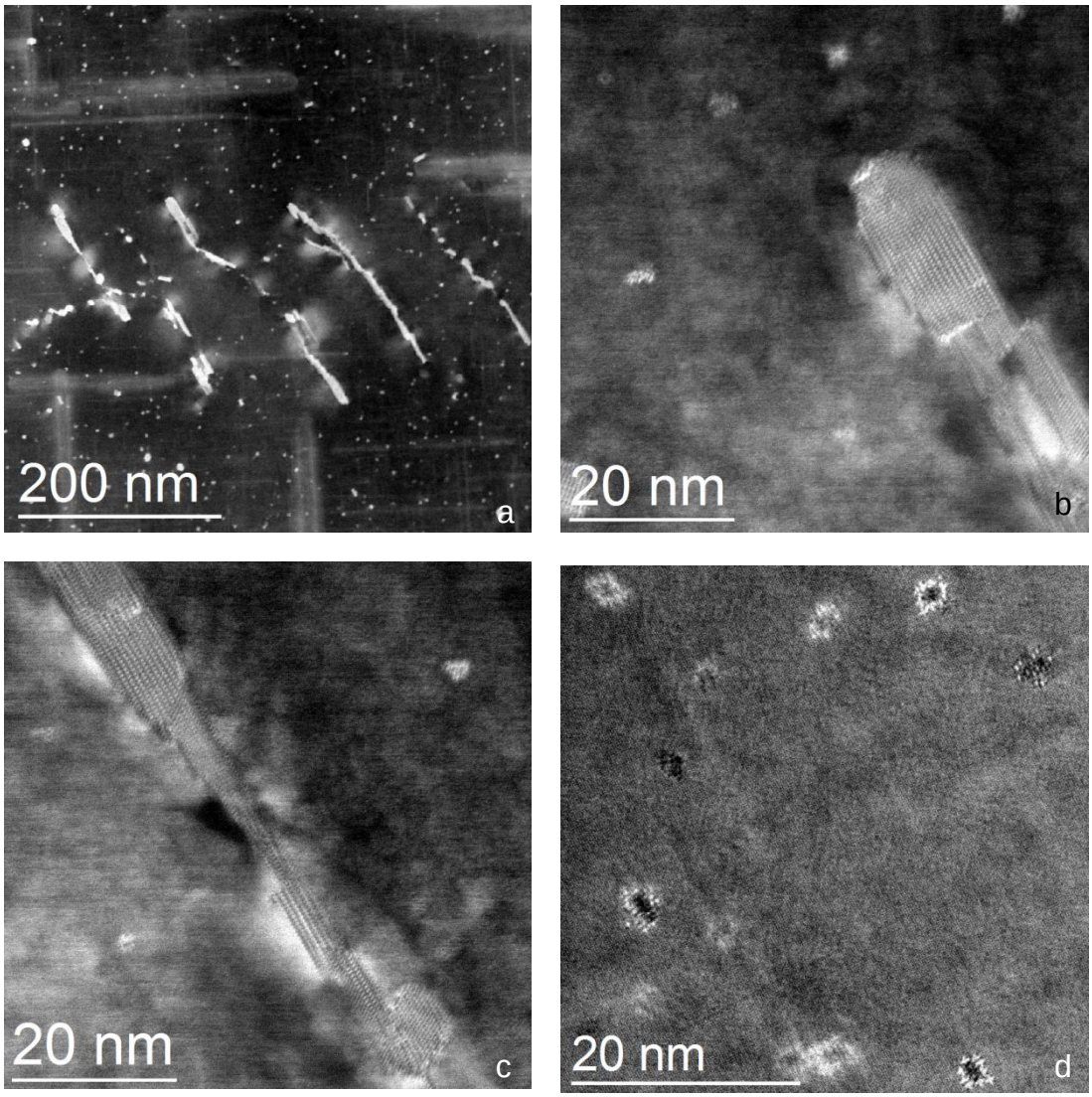

Figure 26: AA2618 T6 prepared with Electrolyte 2, (TITAN, 60 kV, 20 V) (a) Gatan HAADF, (b) Gatan ADF, (c) Gatan ADF, (d) FEI HAADF

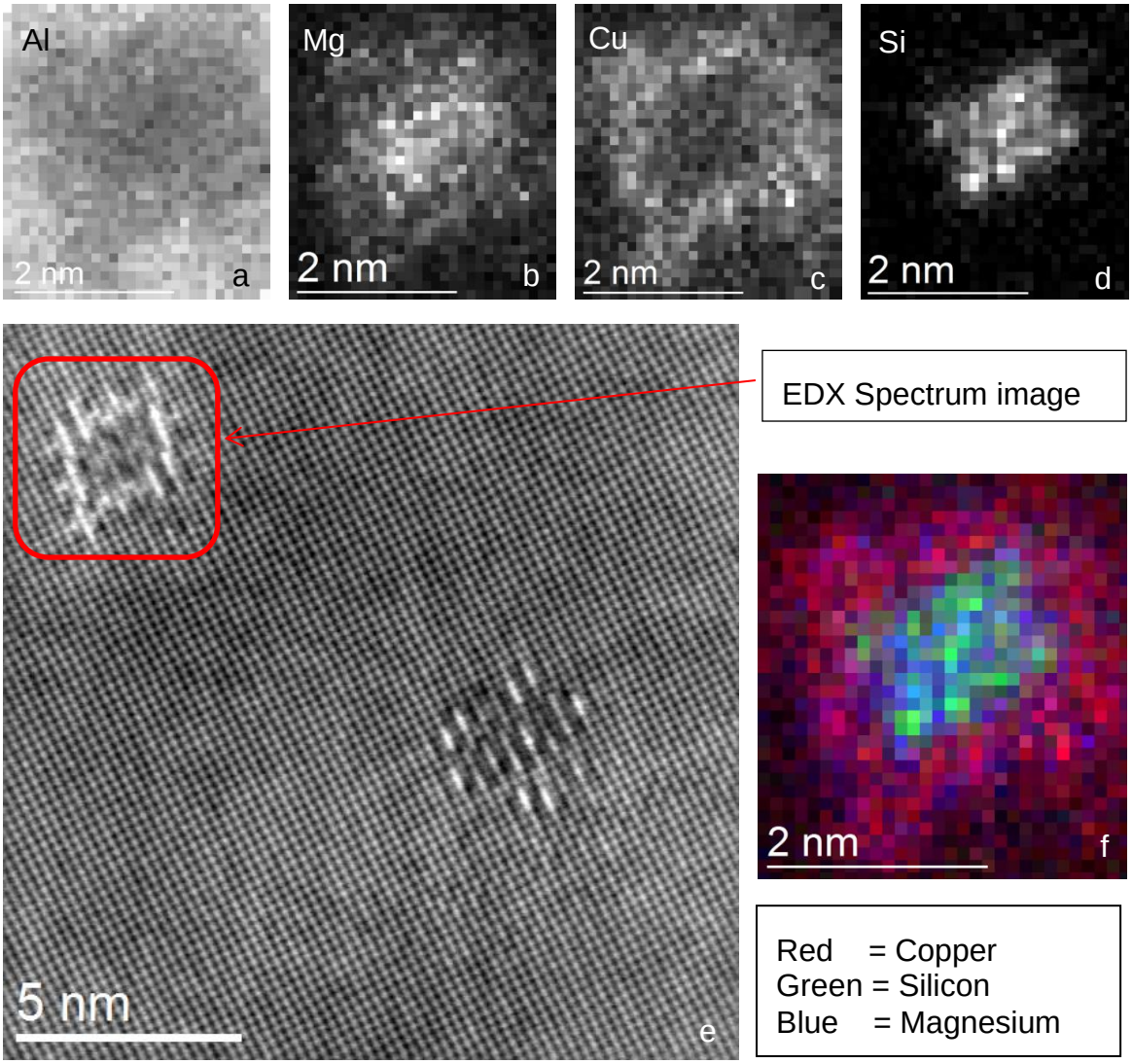

Figure 27: AA2618 T6 prepared with Electrolyte 2, (TITAN, 60 kV, 20 V, STEM camera length 73) (a) EDX Al–Signal, (b) EDX Mg–Signal, (c) EDX Cu–Signal, (d) EDX Si-Signal, (e) FEI HAADF HR TEM and (f) RGB composite of the EDX signals

This sample prepared at 20 V and post treated with the PIPS is the best one we achieved. High resolution imaging and the analysis of small particles were possible. However, to find another electrolyte whereby no PIPS post treatment is necessary more electrolytes were tested.

Preparation with Electrolyte 3

This electrolyte was chosen from an electrolyte list given for the electro polisher by the Fischione Company [39]. The preparation took place at a temperature of -10°C and a voltage of 10 V. Because better results were achieved at a lower temperature,

the recipe was cooled down to -20°C. The flowrate was set to 13 and the voltage varied between 10 V and 35 V with steps of 5 V. The detailed preparation parameters are given in appendix (aluminium preparation experiment 11). The followed OM investigations showed the numbers of the holes varied between one big hole and many small holes. As investigated on the AA2016 sample series with electrolyte 3 the sample surfaces changed from wrinkled to smooth at voltages higher than 20 V. All samples were investigated in CM20 at 200kV.

Figure 28 shows BF images of each voltage step. The surfaces of the samples with 10 V (Exp. 11, a167), 15 V (Exp. 11, b171) and 20 V (Exp. 11, c168) look more etched than polished. This shows that the voltage was too low, so that an etching process instead of polishing happened (figure 3). Better results were obtained with voltages starting with 25 V (Exp. 11, d164). These three samples (25 V, 30 V, 35 V) were prepared in the polishing regime. All three samples had thin areas, but the sample with 30 V (Exp. 11, e172) has in comparison to the other two samples (Exp. 11, d172 and f160) less electron thin areas.

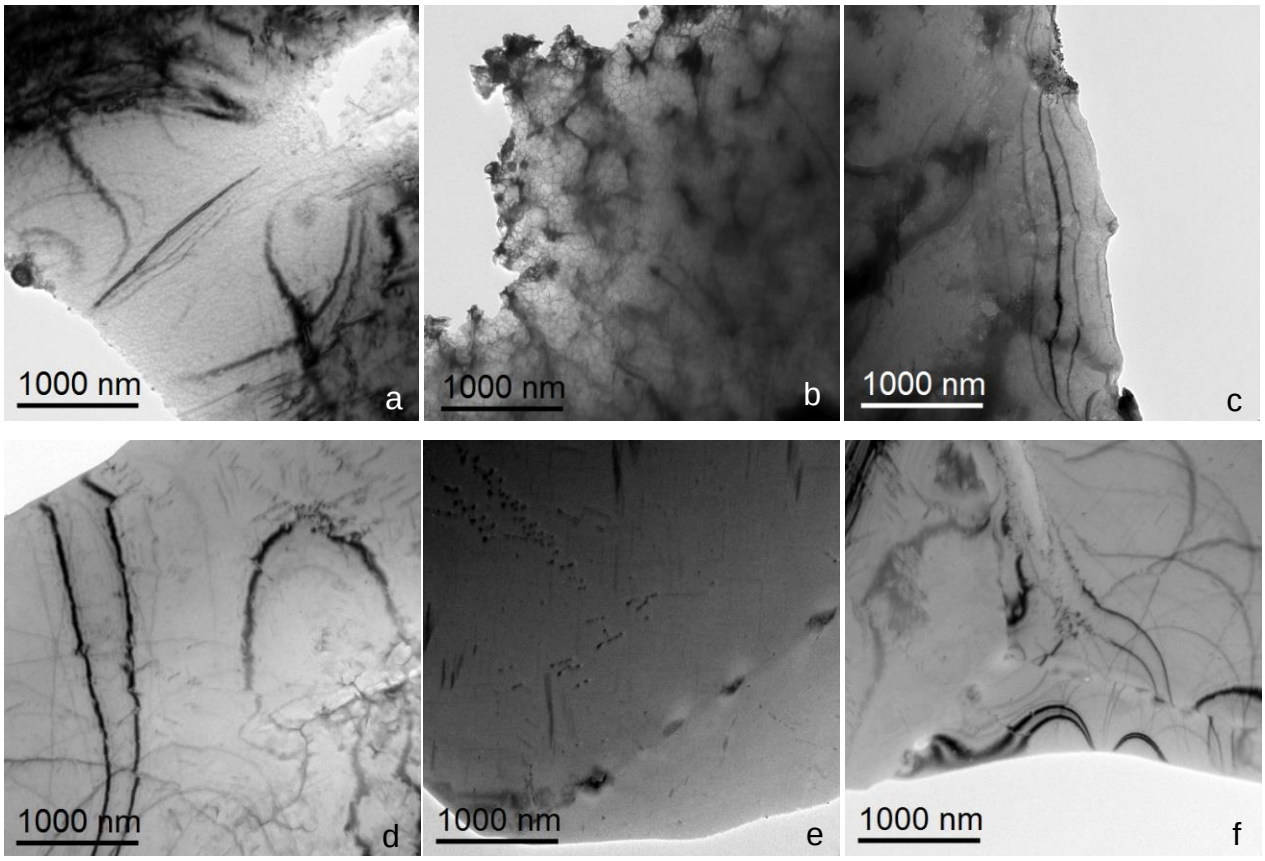

Figure 28: AA2618 T6 prepared with Electrolyte 3, (CM20, 200 kV, BF TEM) (a) 10 V, (b) 15 V, (c) 20 V, (d) 25 V, (e) 30 V and (f) 35 V

This electrolyte appears promising, because the surface looks smooth and the structure (e.g. grain boundaries) of the material is also visible. In order to reveal the perfect voltage, another preparation series was done. The voltage was varied between 23 V and 40 V with steps of 2 V and 3 V (Appendix: Aluminium preparation Experiment 14).The sample, which was prepared with 23 V (Exp. 14, a151) shows an etched surface (Figure 29 a), like the first samples from figure 28. Preparations with voltages between 25 V and 40 V happen in the polishing regimes, which figure 29 b-c illustrates. Based on the CM20 pictures and investigations, a preparation with a voltage between 35 V and 38 V would be recommended. For more precise information about this electrolyte investigations at higher magnifications are necessary

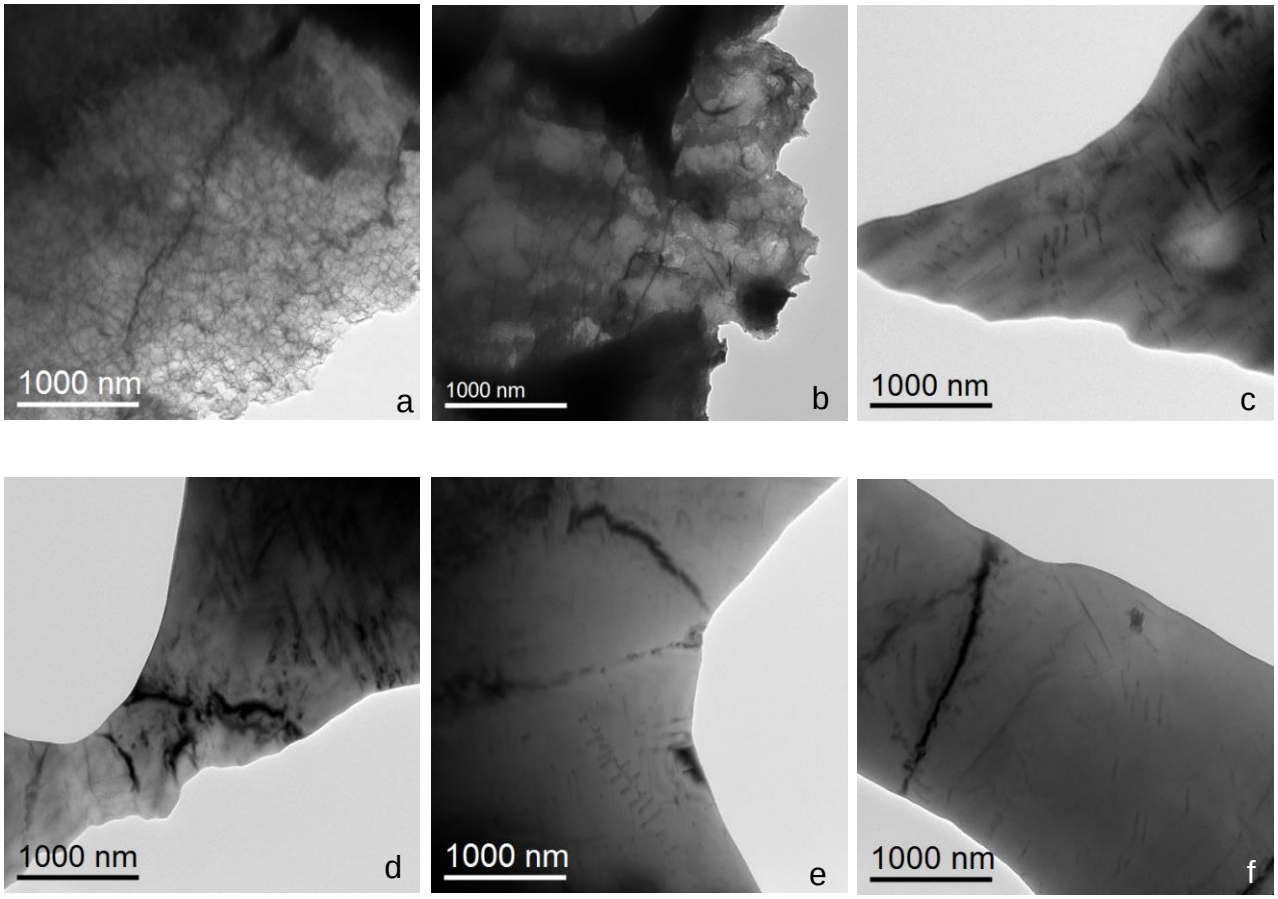

Figure 29: BF TEM of AA2618 T6 prepared with Electrolyte 3 (2nd preparation series), (CM20, 200 kV) with (a) 23 V, (b) 28 V, (c) 33 V, (d) 35 V, (e) 38 V and (f) 40 V

Preparation with Electrolyte 4

The electrolyte number 4 was used for the preparation of samples from cast aluminium alloy from Wiengmoon et.al. [40]. The preparation was performed at -20°C and with a flowrate of 13. The voltage was varied between 15 V and 40 V with steps of 5 (see appendix: aluminium experiment 13). As seen in the Figure 30 (Exp. 13, a160, b156, d157, f160) a preparation with these preparation parameters was not possible. More intensive test series with variation of the flowrate, temperature and voltages are needed, for more precise information about this electrolyte.

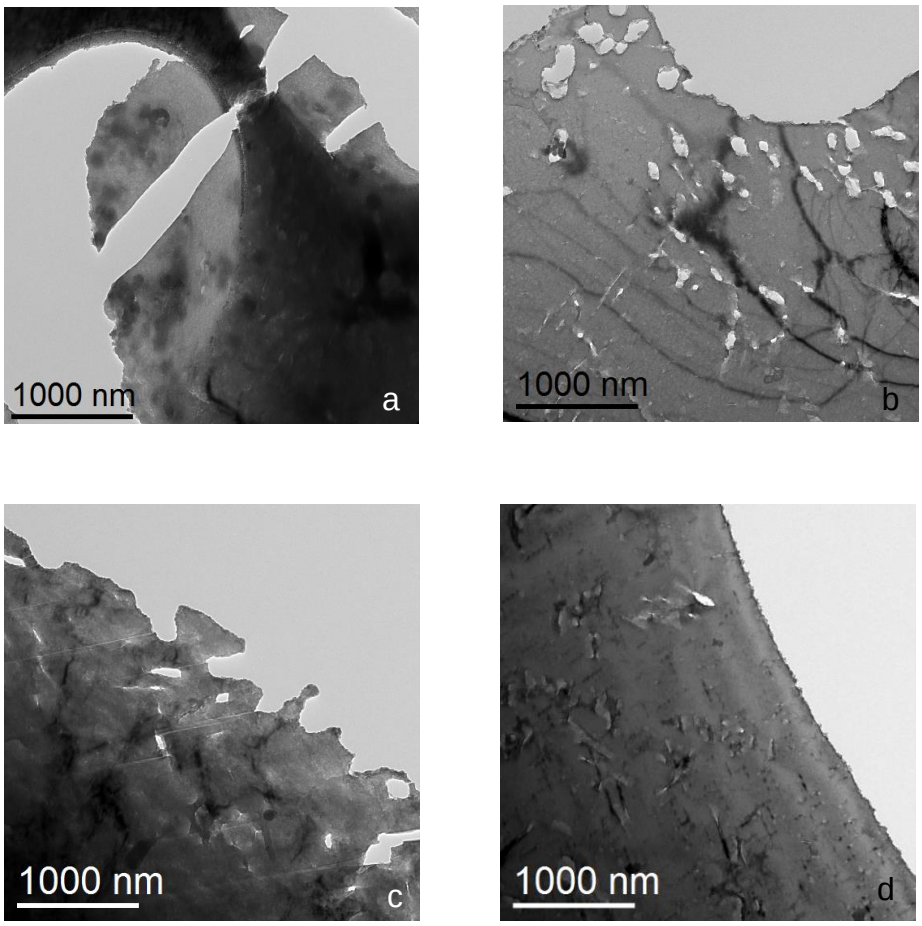

Figure 30: BF TEM of AA2618 T6 prepared with Electrolyte 4 (CM20, 200 kV) with (a) 15 V, (b) 20 V, (c) 30 V, and (d) 40 V

Argon ion milling (PIPS) preparation

To draw comparisons between electropolished and only PIPS prepared samples, sample AA2618 T6 was prepared first with 4 kV and second with decreasing voltage from 4 kV to 2 kV. These preparations were done by Manuel Paller.

Both specimens had a thickness of about 150µm before the final mechanical polishing. Then the samples were dimpled from one side to a thickness of approximately 16 µm. The first sample was inserted into the PIPS and polished by using gun energy of 4 keV. The right gun, shot within an incident angle of 4° parallel to the sample surface from above and the left ion gun within an incident angel of 6° from below. The preparation ended after the resultant hole was visible with the observing system on the PIPS. The second sample was first thinned with 4 keV under the same incident angles as above until a hole was produced (after 4 h). The ion energy was then reduced to 2 keV (for 2 hours) for broadening the hole smoothing the sample surface and production of wider thin areas.

The first sample was investigated with TF20 at 200 kV. Figure 31 shows wide thin areas, but not homogeneously thin.

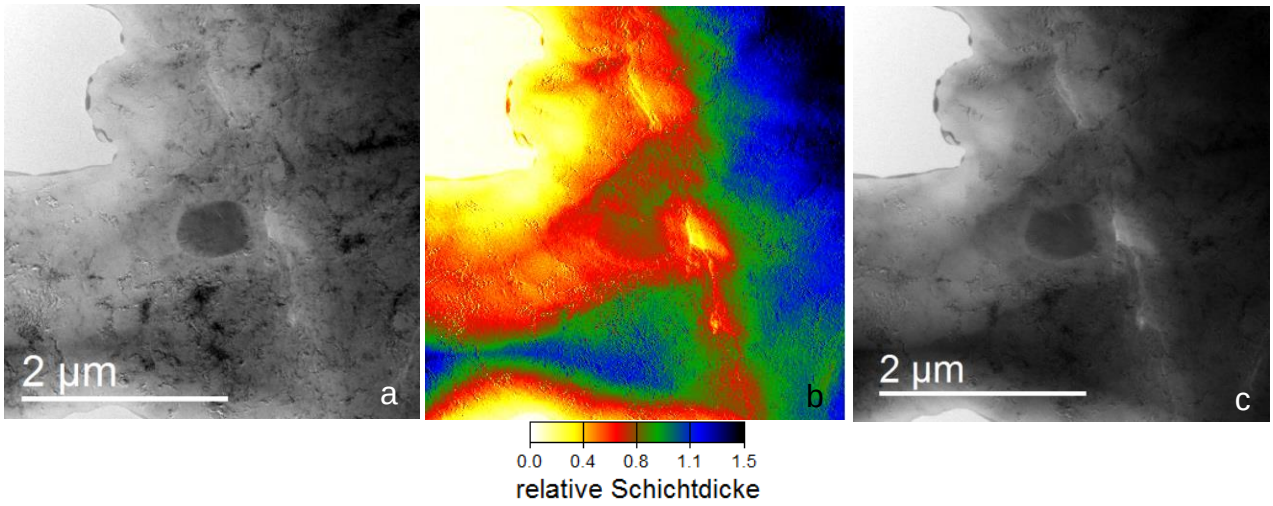

Figure 31:AA2618 T6 with PIPS 4 keV prepared sample (TF20, 200 kV) (a) BF TEM, (b) thickness map (t/λ) and (c) ZL BF TEM

The second specimen, which was prepared with 4 keV and 2 keV, was investigated in CM20. The electron thin areas are wider and more homogeneous, compared to the first specimen (Figure 32). This preparation is to prefer, because the sample is clean with uniformly thin areas around the hole

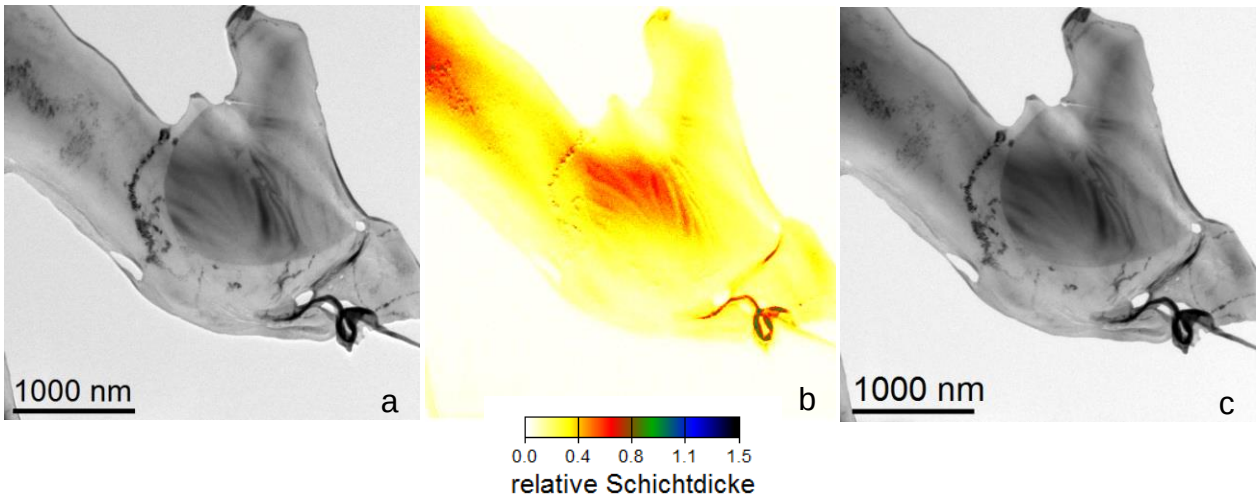

Figure 32: AA2618 T6 with PIPS 4/2 keV prepared sample (CM20, 200 kV) (a) BF TEM, (b) thickness map (t/λ) and (c) ZL BF TEM

This specimen was further used in the following plasma cleaner tests for verifying the opportunity to improve the sample quality. This is described in the subchapter 5.2.4.

5.2.3 $AlCu_4Ti_{0.2}$ T6

$AlCu_4Ti_{0.2}$ T6 was prepared only once with the electrolyte 3 based on the promising results obtained for alloy AA2618 T6. The used parameters were: a temperature of -20°C, flowrate 13 and the voltage was varied between 20 V and 35 V by alternating steps of 3 V and 2 V (appendix, aluminium exp. 15). The following pictures of CM20 (figure 33) show the etched surface of the sample with 35 V (Exp. 15, g166) as general example of the preparation series. The results show, that the preparation regime worked in the etching area instead in the polishing. A variation in the polishing parameter could improve the sample quality and should be investigated with further test series.

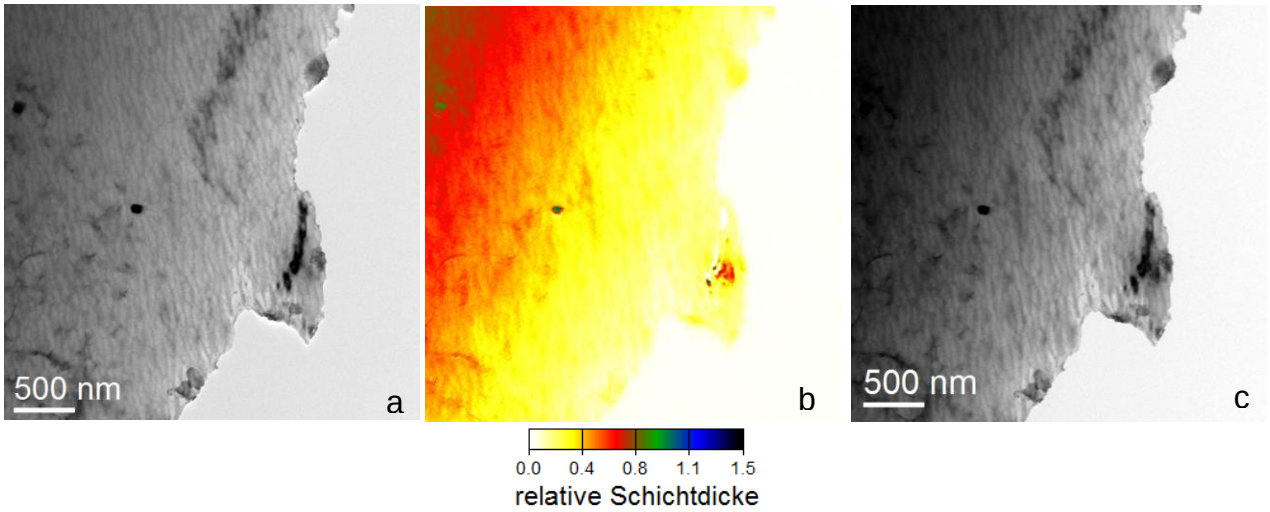

Figure 33: $AlCu_4Ti_{0.2}$ T6 prepared with electrolyte 3, 35 V (CM20, 200 kV) (a) BF image, (b) thickness image (t/λ) of BF and ZL BF images and (c) ZL BF image

5.2.4 He/Ar Plasma cleaner test

The plasma cleaner procedure has been checked since Isabell et.al. [34] describes it as a very efficient method for amorphous layer removal. The main idea was to find an alternative post treatment to PIPS, with a lower removal rate. Two experiments were performed, in order to investigate if an obvious influence on the surface of our samples happens. The used gas mixture contained 20% argon and 80% helium [35]. A conventional gas mixture (20% oxygen/ 80% argon) cannot be used for aluminium and magnesium samples, because of the high oxidation rate of these materials. One sample was prepared by PIPS ion milling (AA2618 T6) and the second sample was prepared with electrolyte 1 and subsequent PIPS treatment (AA2016). Both samples were investigated in CM20 before and after both plasma cleaner treatments. The time spent by the samples inside of the plasma cleaner ranges from 2 to 10 minutes of each treatment. Little changes of the material were observable but not documentable. Thus, further experiments for setting the correct plasma cleaning parameters followed by high resolution investigations with TEMs are recommended.

5.3 Preparation and investigation of Eco AM50 magnesium-alloy

For the preparation of Eco AM50 magnesium alloy six different electrolytes (table 8), cryo-microtomy and Focused Ion Beam preparation followed by low energy argon ion milling (NanoMill), and PIPS thinning under cryo conditions (stage temperature -20°C) were tested.

In the following sub-chapters the detailed preparation and the results are documented.

Table 8: List of the used electrolytes

Electrolyte	Composition
1 [40]	7.9g LiCl 16.8g Mg-perchlorate 750ml Methanol 150ml 2-butoxy-ethanol
2 [41]	250ml $HClO_4$ 750ml Methanol
3 [37]	330ml HNO_3 670ml Methanol
4 [38]	100ml HNO_3 900ml Methanol
5 [42]	50ml $HClO_4$ 600ml Methanol 350ml Butanol
6 [43]	50ml $HClO_4$ 950ml Ethanol

5.3.1 Eco AM 50 with Electrolyte 1

The first electrolyte was mentioned by Dr. Jiehua Li from Montan University of Leoben. He recommended the electrolyte, the voltage (24 V) and the temperature (-40°C). The first preparation series with this electrolyte was at 22°C to test the electrolyte and to determine how the specimen looks like. The flowrate was varied between 10 and 20 in steps of two. The second experiment series was done with the same voltage (24 V), with flowrate 13 and a temperature around -37°C. The reason, why the flowrate 13 was chosen is that there was no significant difference between the originated sample hole size and edge structure and the pre-set standard flowrate at the device is 13. The electrolyte was cooled with dry ice before and during the preparation. The detailed parameters are given in the appendix (AM50, experiment 1 + 3). Directly after the preparation all specimens were washed with Methanol in three glass dishes, to remove the electrolyte.

The samples from experiment 1 were only investigated with the OM, in order to visualize the surface and the hole – distribution. Figure 34 presents OM images (a-d transmitted light and a'-d' incident light images) of samples prepared with different flowrates. Their surface is uneven and the holes are small.

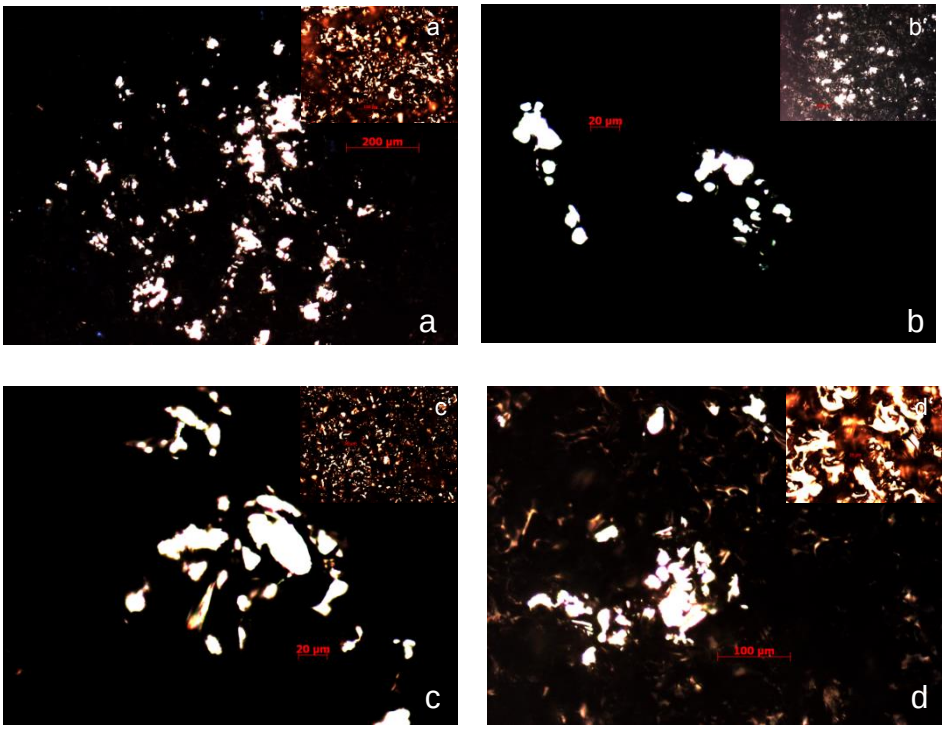

Figure 34: OM images of Eco AM50 with electrolyte 1(first preparation) (a) flowrate 10, (b flowrate 12, (c) flowrate 14, (d) flowrate 16

The specimen from experiment 3 shows that the samples surface was also at this temperature uneven and the originated holes too small, thus all samples got a post treatment in the PIPS at 4 keV (angle right gun: 4° from above, angle left gun: 6° from below) Figure 35 (Exp. 3, b) demonstrate a representative sample for the experiment series 3.

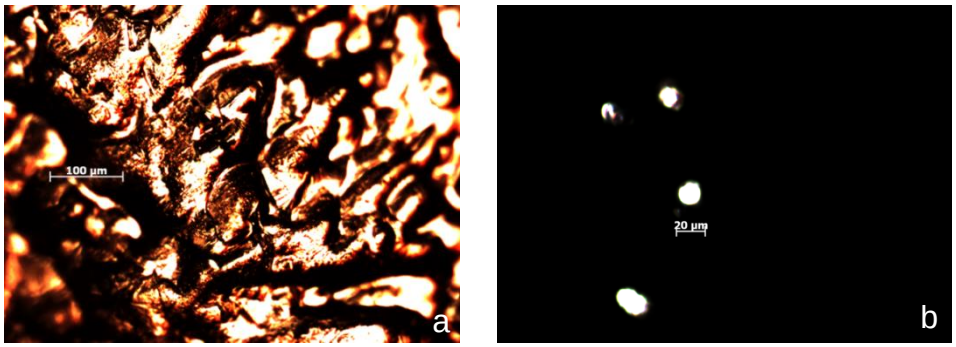

Figure 35: OM (a) incident light and (b) transmitted light image of Eco AM50 with electrolyte 1 (second preparation)

One sample (see appendix: Eco AM50 experiment 3, sample d) was then investigated at TF20 at 200 kV. The surface appears etched although the area would be thin enough for investigations (Figure 36).

Even after the PIPS treatment, etching artefacts are visible (Figure 36), and during high resolution imaging recrystallization occurs under the electron beam exposure. This phenomenon was recorded and is visible in figure 37. This indicates that the specimen is highly beam sensitive and lower acceleration voltages are needed for the following HRSTEM investigations. In all subsequent experiments the samples were pre-investigated with CM20 at 200 kV onto electron transparent areas and those, which appear suitable, were investigated at TITAN with 60 kV.

The samples were stored in methanol after the preparation to avoid sample oxidation.

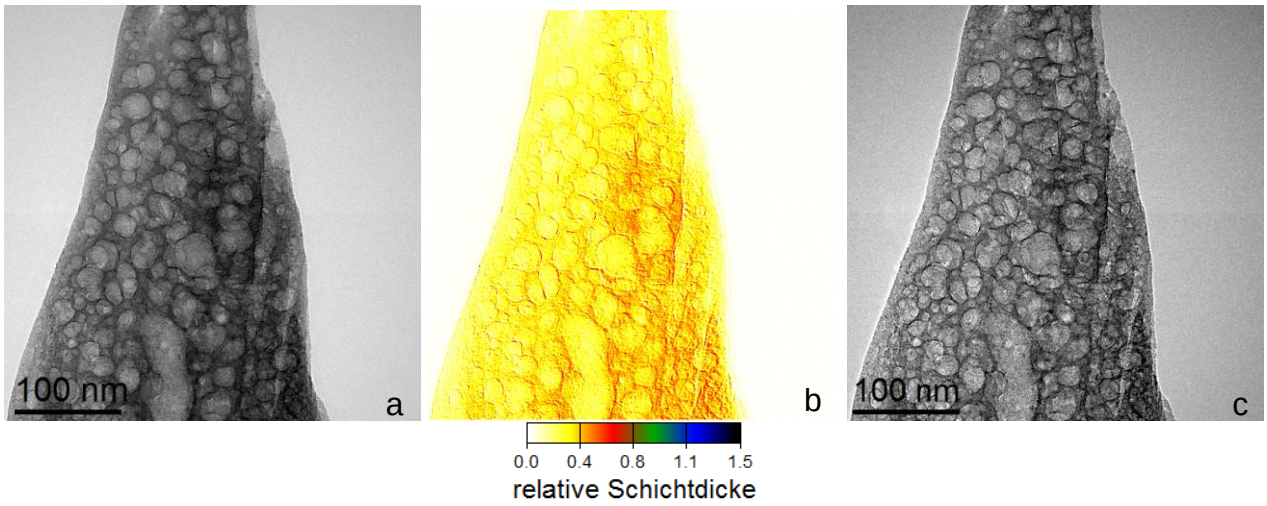

Figure 36: Attacked surface and thickness image, TF20 images of Eco AM 50 (Electrolyte 1 at minus 37°C +PIPS), (a) ZL BF TEM image, (b) t/λ – image, (c) BF TEM image (200 kV)

The preparation with these parameters did not suit for Eco AM50; also the post-treatment with PIPS was too short to remove the etching artefacts. More testing series with voltage variations are recommended for future experiments.

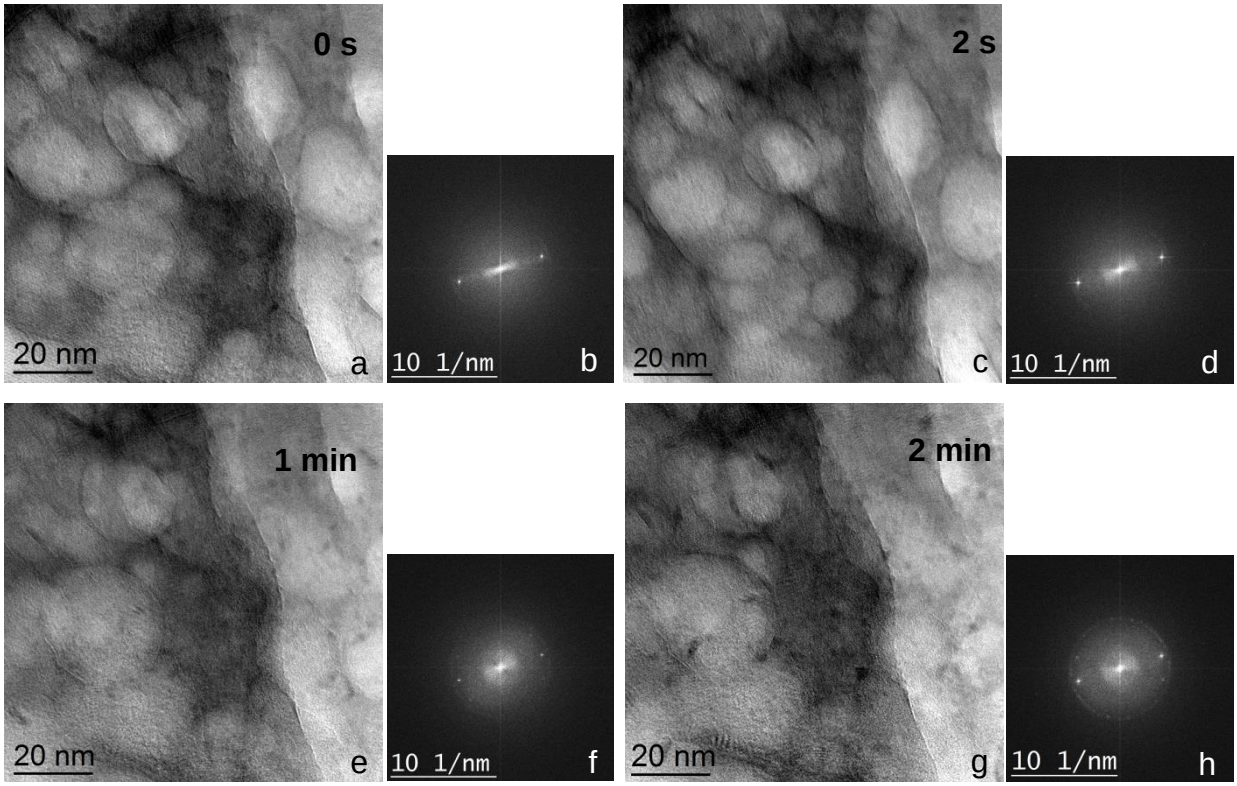

Figure 37: Recrystallization due to electron beam sensitivity, TF20 HR TEM images and FFT-images of Eco AM50 after (a, b) 0sec, (c,d) 2 sec, (e,f) 1 min and (g,h) 2 min exposure time (200 kV)

5.3.2 Eco AM 50 with Electrolyte 2

The second electrolyte was also from Dr. Jiehua Li, who mentioned it in a paper [42].

The given parameters are 20 V and -40°C as the temperature for the electrolyte. The first preparation series was done at -15°C to -10°C, the electrolyte was over the night in the freezer and this is the maximum temperature which can be achieved. During the preparation, the flowrate was varied again between 10 and 20 by steps of two. All of the prepared specimens were investigated with the OM in order to control the surface quality.

The second preparation series was done again with 20 V and -40°C as electrolyte temperature (cooled with dry ice) and with flowrate 13 (with the same reason as mentioned at 5.3.1). The detail preparation parameters are listed in the appendix (AM50, experiment. 2 and 4).

In figure 38 four in the OM investigated samples with different flowrates are pictured (a-d transmitted light and a'-d' incident light images). They show that the surface appears different as with the first electrolyte prepared samples. The holes are bigger and merged together.

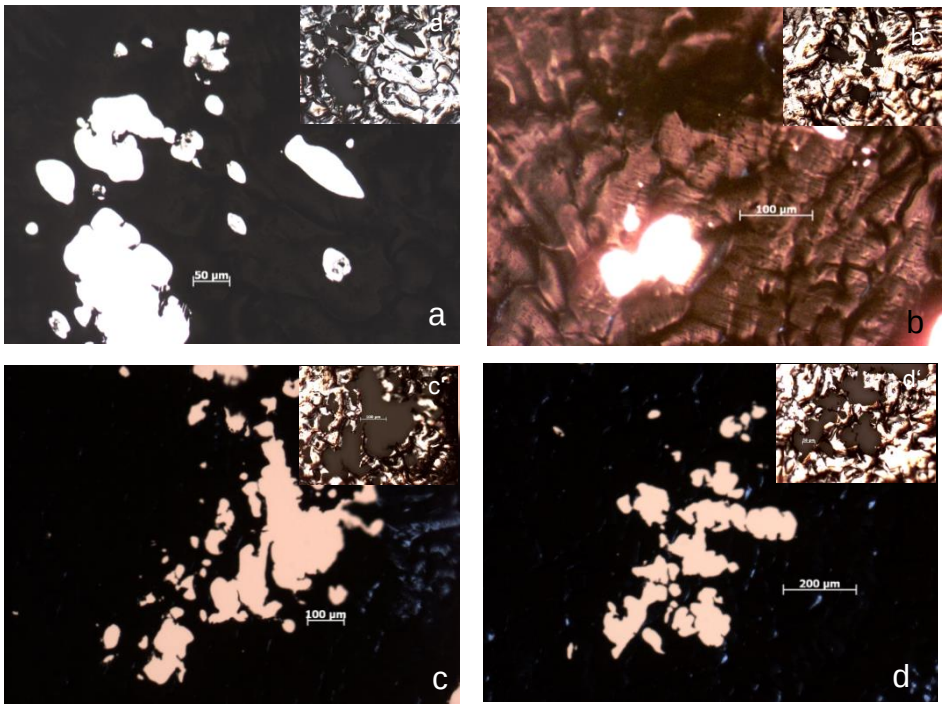

Figure 38: OM images of Eco AM50 with electrolyte 2, (a) flowrate 10, (b), flowrate 12, (c) flowrate 14 and (d) flowrate 16

One specimen of the experiment 4 series, which was performed at -40°C, was investigated at CM20. The surface looked etched and thin areas were hard to find. Some parts were really thick, and the thinner ones are not investigable. In figure 39 a BF and ZL BF image is visible with the relative thickness map. They show thin but damaged parts and thicker (not electron transparent enough) regions, which are not suitable for HRSTEM investigations.

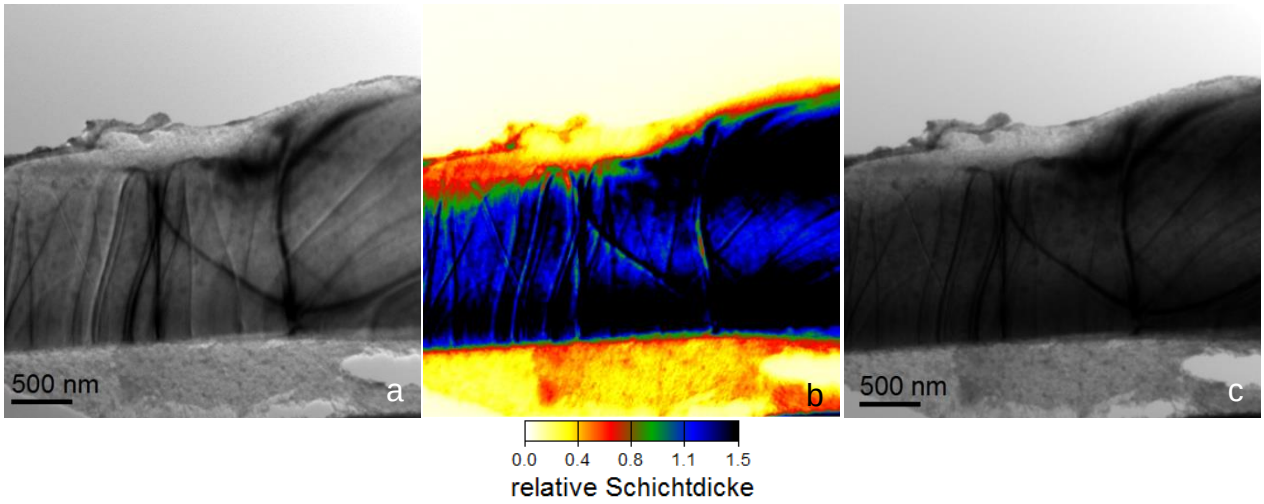

Figure 39: Attacked surface and thickness image, CM20 images of Eco AM 50 (Electrolyte 2 at -40°C, 20 V), (a) BF TEM image, (b) t/λ – image, (c) ZL BF TEM image (200 kV)

The specimens of the second preparation series were stored in methanol and one of them was stored in liquid nitrogen for later investigations. The sample, which was stored in liquid nitrogen, was investigated at TF20 with a cryo-TEM holder. By reason of the frozen liquid film on the surface no imaging and analyses were feasible. To determine suitable preparation parameters more detailed experimental recommended.

5.3.3 Eco AM 50 with Electrolyte 3

The third electrolyte is identical to electrolyte 2 from the aluminium alloy preparation procedure. The parameters were: flowrate 13, temperature -40°C and the voltage was varied between 10 V and 35 V by steps of 5 volts. Those specimens were kept in methanol for the transport to the TEM and immediately investigated at CM20. Details of the preparation are given in appendix (AM50, experiment 5).

As visible in figure 40 some thicker areas, of another phase than matrix, look like fingers, since the surrounding thin areas (probably matrix) are all etched away. The phenomenon of selective etching occurred on all samples of this experiment series.

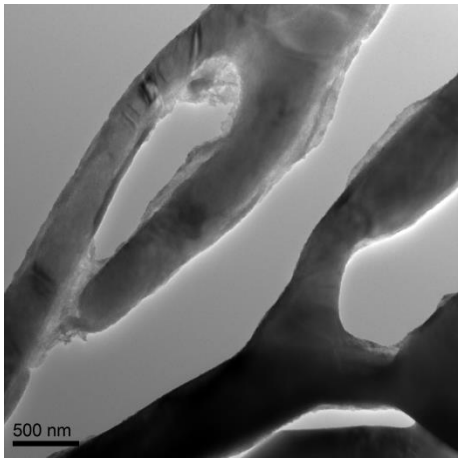

Figure 40: Eco AM50 "Fingers"; Electrolyte 3, 20 V; CM20 (200 kV) BF TEM

The sample, which was prepared with 10 V (Exp. 5, a148), was investigated at the TITAN with 60 kV and 45 pA. Although the sample was beam sensitive, precipitates in the matrix were still visible and with EDX investigable. But after the measurement the area was damaged. In the figures 41 and 42 EDX analyses from a small precipitate and from the "fingers" are seen. The small precipitates contain a high amount of copper besides magnesium and also a little bit of calcium. The composition of the "fingers" consists of a higher amount of aluminium and calcium, than magnesium.

Further experiments with varying parameters are recommended to improve the samples surface quality.

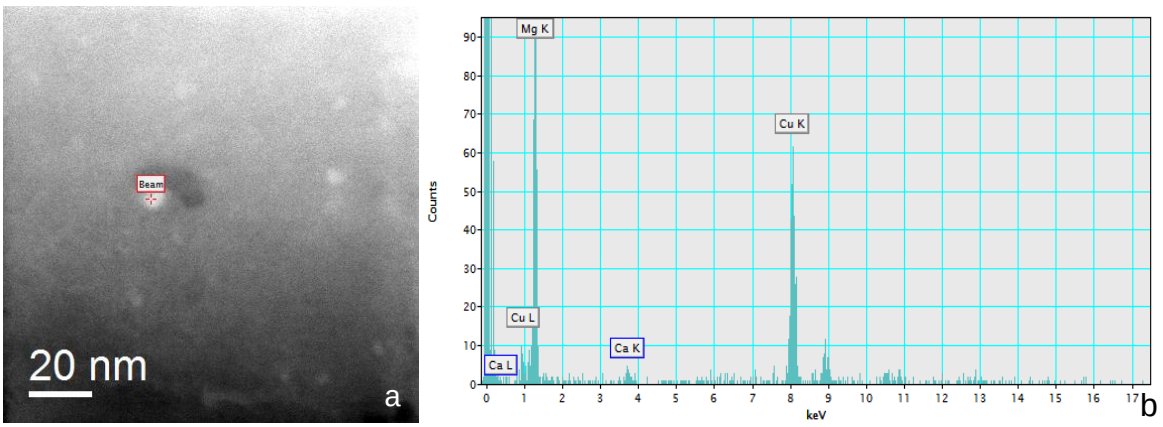

Figure 41: Small precipitate (FEI HAADF) with EDX analysis (Eco AM50 electrolyte 3, 10 V, TITAN at 60 kV, 45 pA, STEM camera length 73)

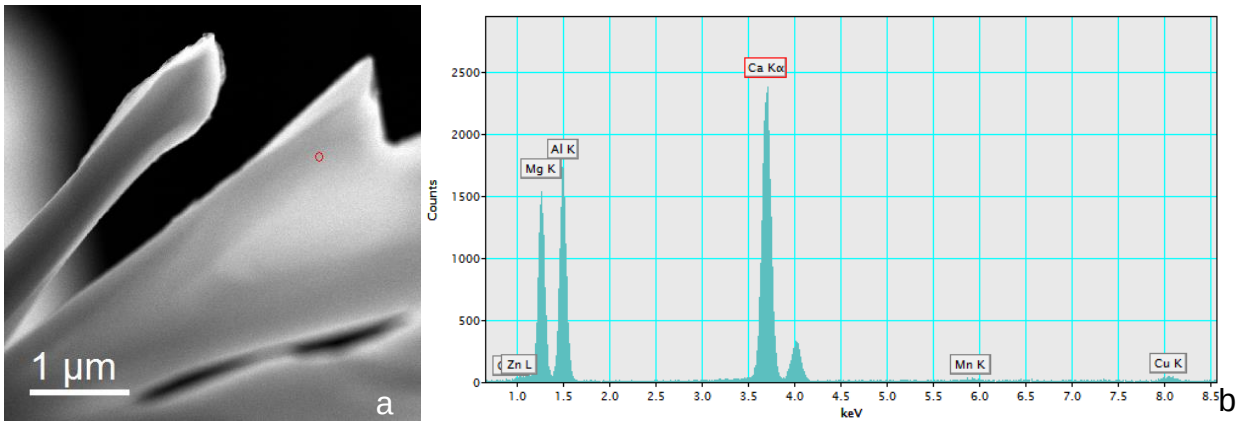

Figure 42: "Fingers" (Gatan HAADF) with EDX analysis (Eco AM50 electrolyte 3, 10 V, TITAN at 60 kV, 45 pA, STEM camera length 73.0)

5.3.4 Eco AM 50 with Electrolyte 4

The fourth tested electrolyte is the same as for the aluminium preparation experiment with electrolyte 3. This electrolyte was chosen; because the amount of the ammonium is less than in the previous used electrolyte 3 and the idea was, that maybe the selective etching effect would be reduced. The parameters for this preparation are the same as for electrolyte 3 (flowrate 13 and temperature -40°C) and the voltage varied between 10 V and 35 V in steps of 5 V. Details of the preparation are given in appendix (AM50, experiment 6).

Those samples were investigated in Titan at 60 kV. All samples shows only etched not polished surfaces with rarely thin areas. The sample prepared with 15 V (Exp.6 b168) looks best of this experimental series and is used to document the typical etched surface (figure 42b) and the sensitivity under the electron beam although 60 kV as acceleration voltage. In Figure 42a the red arrows show the beam damage after investigation at higher resolution. This electrolyte is not recommended for Eco AM50 alloy preparation.

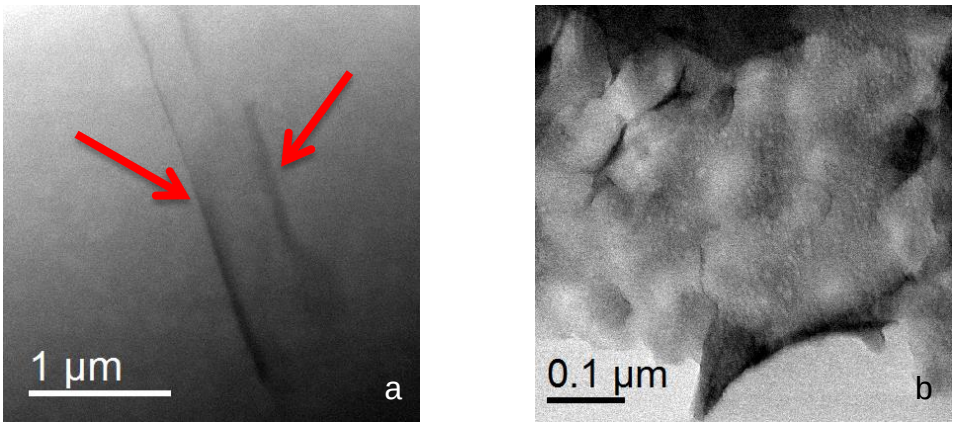

Figure 43: Beam damage (FEI HAADF) and etched surface (Gatan BF-DF) of Eco AM50 electrolyte 4, 15 V (Titan at 60 kV, 80 pA)

5.3.5 Eco AM 50 with Electrolyte 5

The fifth electrolyte was from Y. Guangyn et.al who prepared sample was AZ91 [43]. This preparation was done with two different parameters. The first set of parameters is: flowrate 13, temperature -30°C and with following voltages: 10 V, 15 V and 20 V. The second set was identical to previous only the temperature was set on -40°C. The detailed preparation information is given in appendix (AM50, experiment 7). From those samples which were prepared at -30°C only the sample with 10 V (Exp. 7, a124) was investigable at CM20. The other two samples did not have any thin areas only sharp edges which indicates that the voltage was too high. The surface of the 10 V sample looked damaged so no further investigation was realized (figure 43a).

The sample series at -40°C documented well how important the interaction of the right preparation parameters for a successful electropolishing performance is. Figure 43 a-d demonstrates the polishing result as a function of voltage and temperature. In future investigations this electrolyte should be analysed in more detail to verify the optimal preparation conditions.

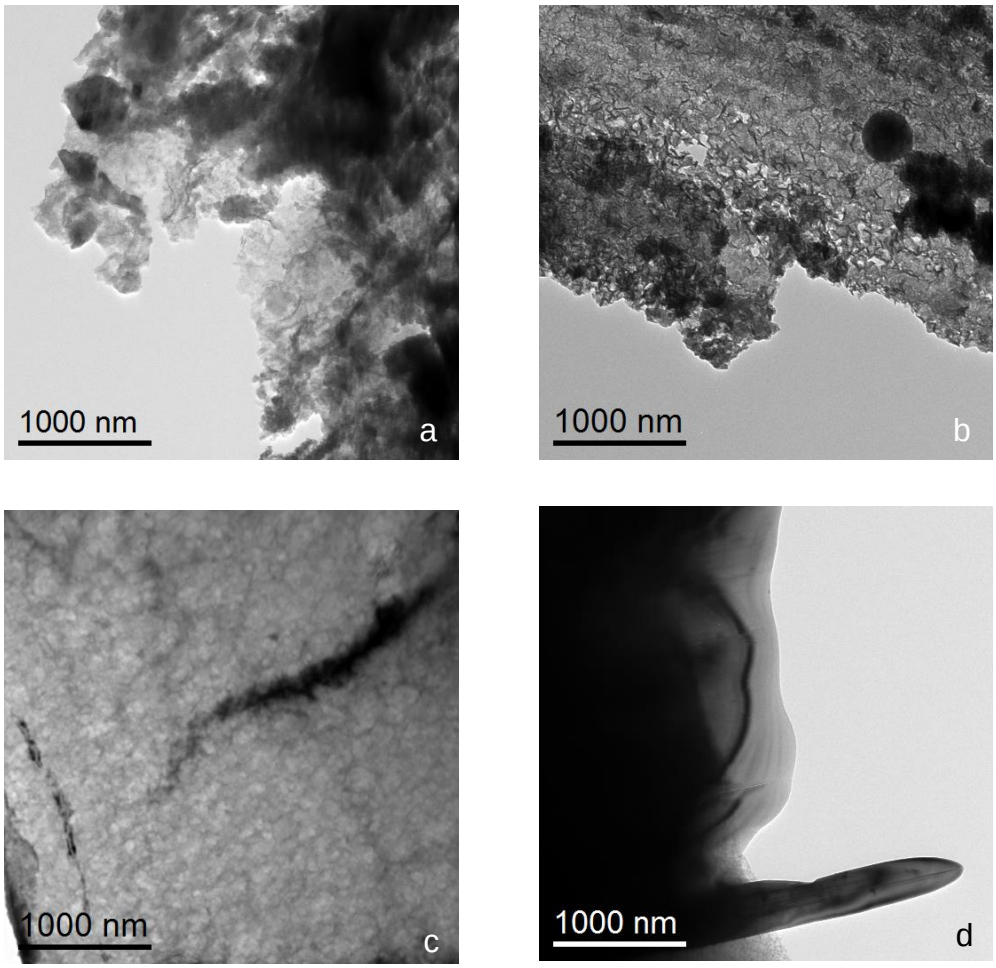

Figure 44: Surface of Eco AM50 (BF TEM), electrolyte 5, (a)-30°C, 10 V, (b) -40°C, 10 V, (c) -40°C 15 V and (d) -40°C 20 V (CM20, 200 kV)

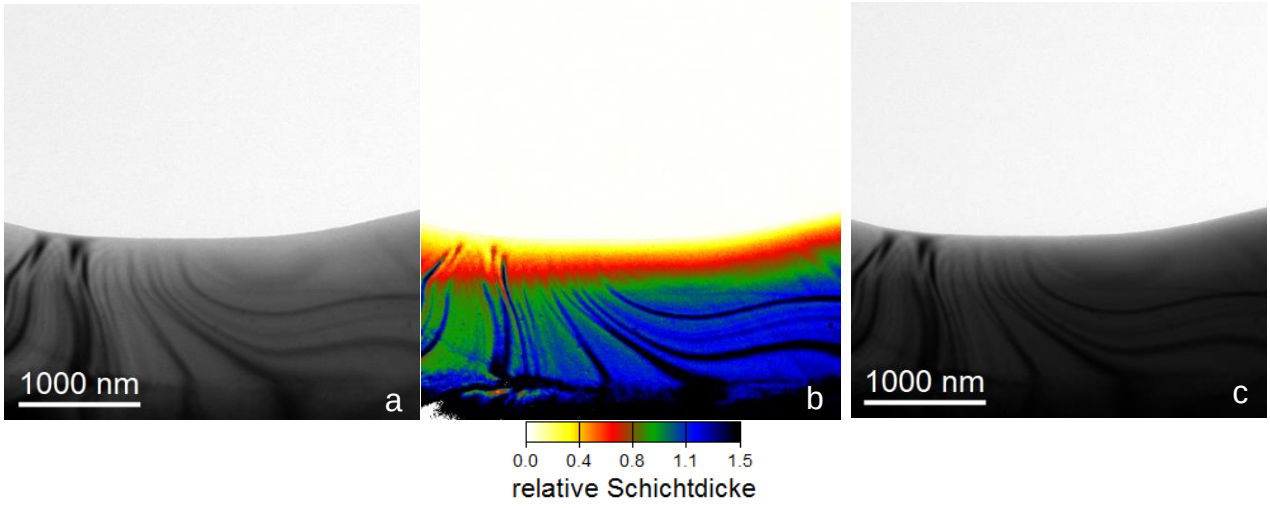

Figure 45: Thinn area Eco AM50 (BF TEM), electrolyte 5, -40°C, 20 V (a) BF, (b) t/λ and (c) ZL BF(CM20, 200 kV)

5.3.6 Eco AM 50 with Electrolyte 6

The last tested electrolyte was taken from Y.D. Huang et.al. who investigated AE42 alloys [44]. The temperature for the preparation was -30°C, the flowrate 13 and the voltage varied from 25 V to 45 V in steps of 5 V (see appendix: AM50, experiment 8).The samples were investigated at Titan with 60 kV. Those samples with a preparation voltage of 25 V (Exp. 8, a154) and 30 V (Exp. 8, b153) were not investigable; the resulting holes were not central on the sample.

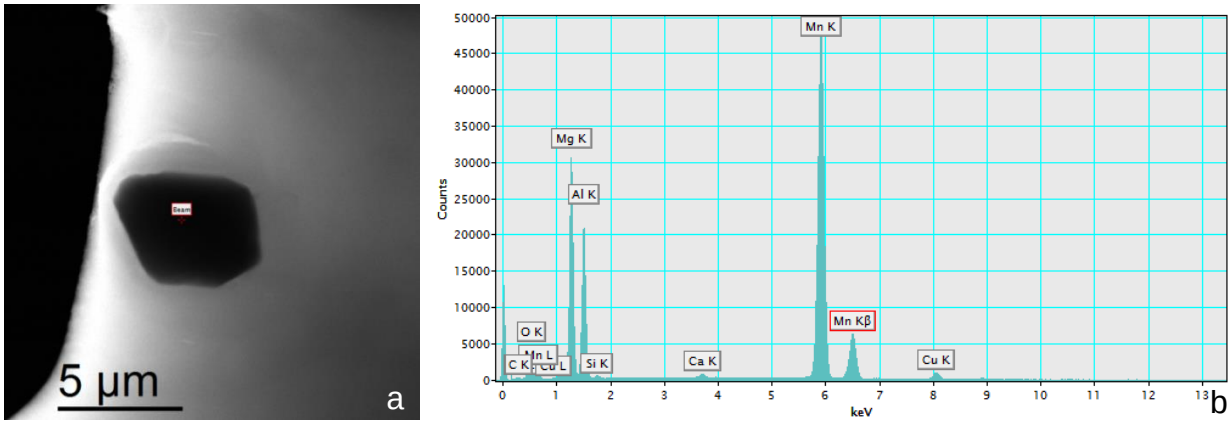

Figure 46: Particle (FEI HAADF) and its EDX spectrum of Eco AM50, electrolyte 6, 35 V (TITAN, 60 kV, STEM camera length 115.0)

The hole of the third sample (35 V, Exp. 8, c147) had thick edges, but some EDX analyses were still possible, e.g. from a manganese rich particle (figure 45) which distinguished clearly from the matrix. The same was also for the last two samples. Selective etching instead of polishing happens; figure 46 shows this situation. The calcium rich zones (“fingers”) are not so strongly affected than the matrix. To obtain the right parameters for the polishing regime, more detail experiments are recommended. Due to lack of time no further investigations were possible.

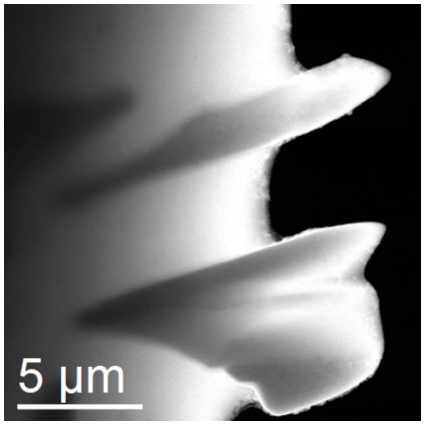

Figure 47: Eco AM50, electrolyte 6, 35V, FEI HAADF image (TITAN, 60kV)

5.3.7 Eco AM 50 with Cryo Microtomy

Since the electropolishing preparation did not work as successful as desired, a cryo–microtome cut under liquid nitrogen was performed. The reason of the usage of liquid nitrogen was to reduce air contact, in order to avoid the formation of an oxidation layer. This preparation was carried out by Ing. Claudia Mayrhofer. This way of preparation was difficult, because the material is brittle and also the cutting diamond knife was damaged. This specimen was investigated in T12 and TF20 microscope under cryo - conditions. Image 47(a) shows an overview of parts of the cut specimen. Due to the high mechanical stress during the cutting, the sample looks ribbed. Figures 47(b) and 47(c) shows a dark-field image of a thin area and its SAED image. These images were recorded at T12 by Dipl. Ing. Dr. Letofsky–Papst.

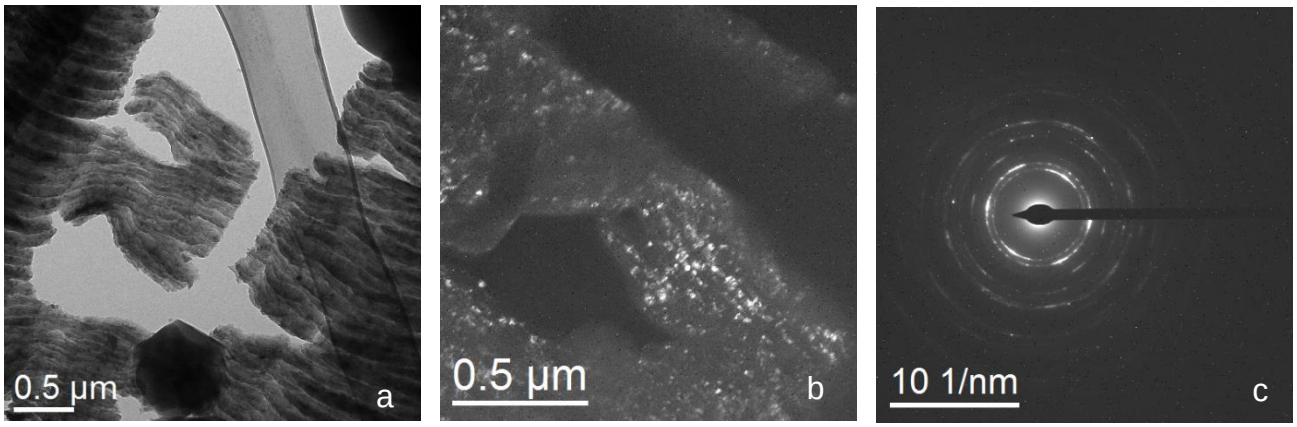

Figure 48: Cryo-microtome cut of Eco AM50 T12 (120kV, cryo conditions) (a) BF TEM (b) DF TEM (c) SAED image of image (b)

The sample shows high crystallinity and no beam sensitivity, so it was further investigated under cryo-conditions at TF20 for high resolution imaging. Figure 48 shows an overview (a) of the characteristic surface and a high resolution image (b) with smaller crystals as aspect. It seems that during the preparation a stress induced recrystallization of the material happened. Based on these results the cryo-microtomy preparation is not recommended but the TEM investigation under cryo conditions should be considered for future analyses.

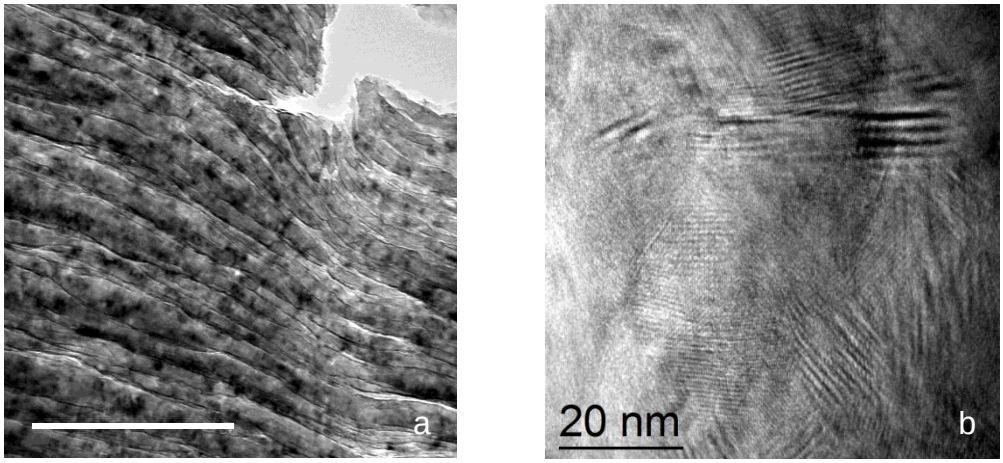

Figure 49: Cryo-microtome cut of Eco AM50 TF20 (200 kV, cryo conditions) (a) BF TEM and (b) ZL HR TEM

5.3.8 Eco AM 50 with FIB and NanoMill

The FIB preparation and the NanoMill post treatment were performed by Martina Dienstleder with the following parameters:

A standard FIB lamella was prepared with “insitu lift out” on an Omniprobe® copper grid. The final thinning was done in three steps, first the lamella was thinned to a thickness of 200 nm with a voltage of 30 kV and a current off 100 pA, with an incident angle of +/- 2° relative to the ion beam. Then a thickness of about 100 nm was reached by using an angle of +/-1° at 30 kV and 50 pA. The last step was used to reduce the amorphous layer with a voltage of 5 kV, an angle of +/-4° and with 70 pA.

A stepwise post treatment performed with low energy focused argon ion milling in the NanoMill at -160°C. After each post treatment the lamella was investigated in TITAN at 60 kV.

NanoMill preparation procedure:

1st NanoMill treatment

Step 1: 10°, 900V, 5 min, 15 x 15 µm over the full lamella

Step 2: -10°, 900V, 5 min, 15 x 15 µm over the full lamella

Step 3: -10°, 500V, 10 min, 15 x 15 µm over the full lamella

Step 4: 10°, 500V, 10 min, 15 x 15 µm over the full lamella

Sample thickness: approximately 100 nm

2nd Nanomill treatment

Step 1: 10°, 900V, 15 min, 15x15 µm over the full lamella
Step 2: -10°, 900V, 15 min, 15x15 µm over the full lamella
Step 3: -10°, 500V, 10 min, 15x15 µm over the full lamella
Step 4: 10°, 500V, 10 min, 15x15 µm over the full lamella
Sample thickness: approximately 70 nm

3rd NanoMill treatment

Step 1: 10°, 900V, 20 min, 15x15 µm over the full lamella
Step 2: -10°, 900V, 20 min, 15x15 µm over the full lamella
Step 3: -10°, 500V, 20 min, 15x15 µm over the full lamella
Step 4: 10°, 500V, 20 min, 15x15 µm over the full lamella
Sample thickness: approximately 50 nm

The surface after the first NanoMill treatment of the lamella was covered with a thick amorphous layer. Moreover, the total thickness of the lamella was in fact not reduced, although it was 30 min inside the NanoMill. It seems that the first treatment was too short so the native oxidation layer originated in the time gap between preparation and NanoMill treatment was not removed. Figure 49 (a) shows a partial overview of the prepared FIB lamella. Recrystallization due to the preparation is already visible in that image. To reduce the amorphous layer the sample was again inserted into the NanoMill for another 50 minutes. The total thickness was thereby decreased to approximately 70 nm. We paid attention that the time on air between NanoMill and TEM investigation was as short as possible so that the native oxidation layer was as thin as possible. To reduce the sample thickness a third treatment in the NanoMill for 80 minutes was done. The total thickness of the lamella could be reduced to around 50 nm but the formation of a native oxide layer could not prevented; consequently only diffuse high resolution images were generated (Figure 49 b,c).

The standard FIB preparation is accordingly to these results not suitable for this alloys, because recrystallization induced during the preparation process have to be avoid. Alternatively FIB preparation under cryogenic conditions or with the interlacing method could bring an improvement in sample quality.

Also the post treatment in the NanoMill needs more effort, to find the right milling conditions for magnesium oxide. Since the parameters were calculated with the milling value of pure magnesium, other specific experiments with magnesium alloys have to be performed. Nevertheless, without the ability to transport the sample under vacuum or inert gas into the TEM, surface oxidation cannot be prevented.

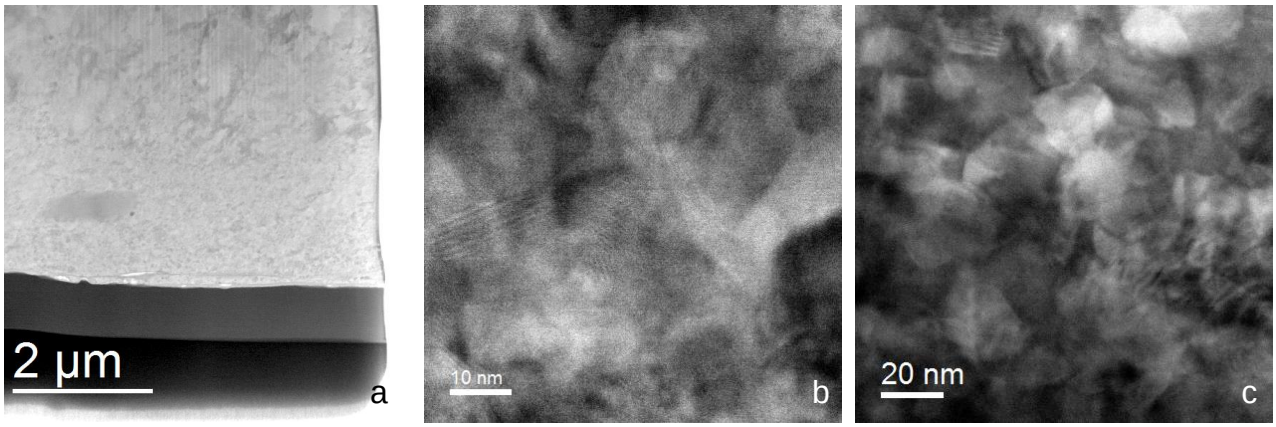

Figure 50: FIB-Lamella of Eco AM50 (HAADF of Titan at 60 kV), (a) after 1st NanoMill treatment, (b) after 2nd NanoMill treatment and (c) after 3rd NanoMill treatment

5.3.9 Eco AM50 with cooled PIPS

The last attempt to prepare Eco AM50 was to use a cooled PIPS preparation. Dr. Jiehua Li from Montan University of Leoben prepared the specimen as follows:
The disc with a thickness of around 150 µm was first thinned carefully to a thickness of 120 µm with a fine abrasive in only one direction. Afterwards it was dimpled from both sites to a thickness of around 15 µm. Then it was given into the PIPS2 device, which has the possibility to cool down the specimen holder to -20°C. With an angle of 10° and a beam energy of 6 keV the specimen was thinned until a hole occurred. Afterwards the angel was reduced to 4° and the energy to 2 keV for broadening the hole and to receive wide thin areas.
After controlling the sample, he brought us the specimen without special transportation conditions (no vacuum, no nonreactive environment) to FELMI and it was immediately investigated in TITAN at 300 kV. The resulting images are

surprisingly good compared to the other preparation methods. The specimen was not as sensitive under the electron exposure as those prepared by electropolishing.
A high resolution image, its FFT and a spectrum image from the same area is shown in image 50 (a) and (b). The area is highly crystalline, and the amorphous layer seems thin enough for high resolution images and analyses. The EDX line scan shows the elemental contribution of magnesium, aluminium and calcium trough the marked area of figure 51(a). The brighter areas in figure 51(a) consist mainly of aluminium and calcium, whereas the two dark straight surroundings consist of magnesium.

These pictures demonstrate that this preparation technique is at the moment best suitable for microscopy investigations with atomic resolution.

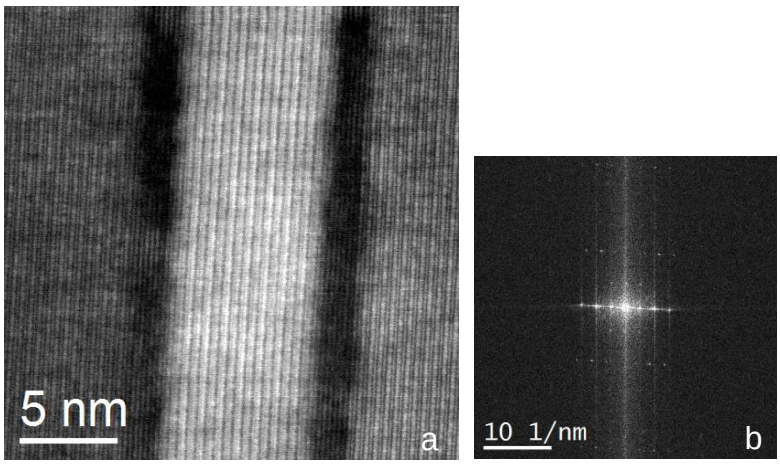

Figure 51: cooled PIPS preparation of Eco AM50, (a) HR TEM (Gatan BF-DF) and its (b) FFT image (TITAN, 300 kV)

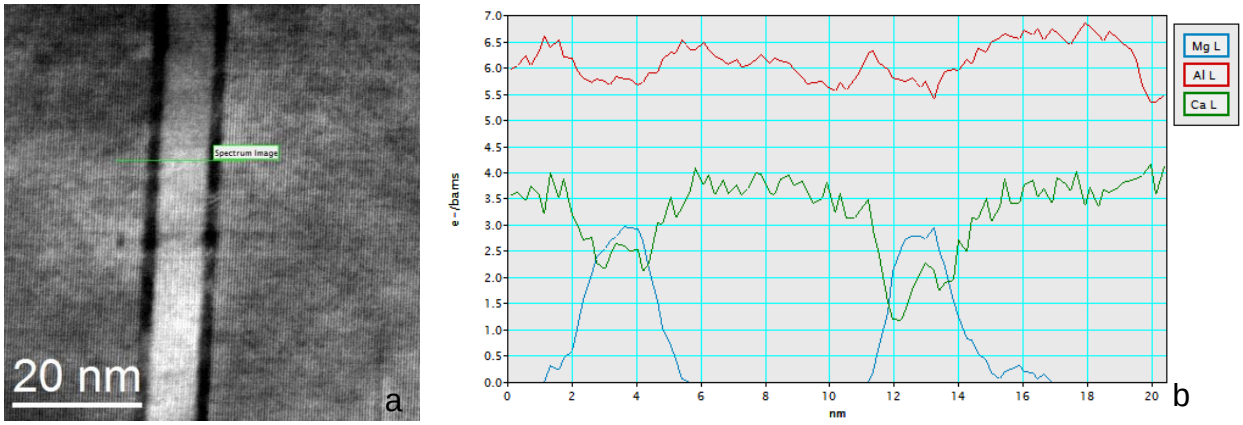

Figure 52: (a) HRTEM (Gatan BF-DF) and (b) its EDX line scan of cooled PIPS prepared EcoAM50 (TITAN, 300 kV, STEM camera length 58.0)

6. Summary and Outlook

Subject of this master thesis was the search for novel, practical ways and recipes for the preparation of transmission electron microscopy samples that are based on aluminium and magnesium. These metals and their alloys are particularly challenging, since sub-optimal specimen preparation has a direct impact on the ability to study the micro or nanostructure as well as the chemical composition, regardless of the particular TEM mode. Hereby, the main focus was laid on electropolishing techniques and on the study of suitable preparation parameters with various electrolytes under different conditions to fabricate suitable, chemically and structurally unaltered, thin TEM samples.

The criteria used to evaluate the preparation quality of the specimens were: size and distribution of resulting holes (OM), relative thicknesses (t/λ) and condition of the surface (etched or polished) (both via TEM). Provided the preparation has passed these criteria, HR-S/TEM imaging, analysing and calculation of FFTs were then performed to determine the presence of amorphous layers and the influence of preparation induced artefacts, like recrystallization.

Several samples, relevant to the context of the OPTIMATSTRUCT project, have been investigated.

For the aluminium alloy type AA2016, a suitable preparation procedure could be determined and consisted a.) of an electrolyte mixture of perchloric acid, distilled water, 2-butoxy-ethanol and methanol and b.) of an ion milling post treatment. This combination brought the best and most reproducible results for high resolution imaging and analysis, with the calculated FFT images, showing the presence of a negligibly thin amorphous layer only (5.2.1). A promising alternative for a procedure without post treatment could consist of a methanol containing nitric acid electrolyte, which would require minor further optimizations for the right etching parameters.

The aluminium alloy AA2618 T6 could be prepared with methanol based electrolytes, containing nitric acid in two different concentrations and one with perchloric acid. Both worked well; however the higher amount of nitric acid still produced some etching artefacts requiring post treatment. In combination with ion milling however, the higher concentration nitric acid electrolyte yielded TEM specimens which are very

suitable for high resolution imaging and analysis (5.2.2) such as samples, fabricated with the electrolyte with less nitric acid and no post treatment.

As a reference for electropolished specimens, a conventionally ion milled sample surface was also generated, yielding large electron transparent areas without any obvious preparation artefacts.

For the preparation of aluminium alloy TEM samples, electropolishing is a promising approach, once suitable parameters are set, with this method fast and high quality samples for high resolution investigations can be obtained.

The preparation process of the magnesium alloy Eco AM50 was impeded by problems that are intrinsic to magnesium alloy: it is very sensitive to ambient oxygen and also to an induced temperature rises during the preparation process. Consequently, all preparation steps had to be carried out in a cooled environment.

The best results were achieved with an electrolyte containing a low amount of perchloric acid, butanol and methanol, resulting in uniformly polished and thin areas good for TEM work. For high resolution, where amphorphization matters more, some of the preparation parameters need to be improved further, if possible at all.

Alternative preparation techniques like cryo microtomy, FIB lamella cutting with a low energy ion milling post treatment and a cooled ion milling preparation with a novel milling device (PIPS 2 ^{TM}) were tested also.

Cryo cut specimens were consequently investigated under TEM cryo conditions also. Although the crystalline specimen was largely stable under the electron beam, the specimens showed strong mechanical compression.

After FIB preparation, due to the rather high milling energy during the last polishing step, samples typically contained amorphous surface layers, which had to be removed by an extra low-energy ion treatment. Samples obtained thereby have been suitably thin, however suffered from massive oxidation during transport from the low-energy milling device to the TEM. In addition, recrystallization processes could be observed during the investigation.

Preparation by ion milling with a cooled stage (PIPS 2 ^{TM}) produced a specimen, which could be directly investigated at high resolution. It was more stable with respect to electron beam damage than electropolished samples. A very thin oxidation

layer, as passive protector layer however was present, despite the fact that the sample was transported under ambient conditions (5.3.9).

One possibility for the overall improvement of sample quality would be the use of low-energy ions directed at the sample, which is cooled at any stage of preparation, as realized with the Ilion^{+TM} device at the FELMI. Although this instrument is dedicated to the preparation of bulk SEM sample surfaces, a clever “misuse” of the device would also allow the preparation of TEM samples, with the advantage to avoid great heat transfer into the material as for FIB samples. Owing to a lack of time, this approach has not been tried but needs follow-up as it entails more gentle conditions.

The preparation of magnesium alloys for TEM remains challenging and requires a more refined combination of electrolytes, as described in chapter 5.3.5 or alternatively preparations under cooling / cryo conditions throughout the whole process.

7. List of Figures

8. List of Tables

9. References

[1] J. Ayache, et.al., “Sample Preparation Handbook for Transmission Electron Microscopy, Methodology”, Springer Science + Business Media, LLC 2010

[2] P.J. Goodhew, “Thin Foil Preparation for Electron Microscopy” from “Practical Methods in Electron Microscopy”, Ed. A.M. Glauert, ELSEVIER, 1985

[3] D.B. Williams and C. B. Carter, “Transmission Electron Microscopy; A Textbook for Material Science”; Springer Scinece + Business Media LLC 1996, 2009

[4] Official project number of COIN OPTIMATSTRUCT funded by FFG: 839083

[5] J. Rees, “Leichtbau, Wie Autos abspecken”, Wirtschafts Woche, 12.12.2012 (http://www.wiwo.de/technologie/auto/leichtbau-wie-autos-abspecken-um-sprit-zu-sparen-seite-all/7489606-all.html) 12.12.2014

[6] Sharmila M. Mukhopadhyay; “Chapter 9: Sample Preparation for Microscopic and spectroscopic characterization of solid surfaces and films” in” Sample Preparation Techniques in Analytical Chemistry”, Ed. by Somenath Mitra; John Wiley & Sons, Inc, 2003; ISBN 0-471-32845-6

[7] Lecture script of Electron microscopy, of Prof. Kothleitner, Semester 2013/2014

[8] D. Landolt, “Fundamental Aspects of Electropolishing,” Review article; Electrochimica Acta. Vol. 32, No1, p 1-11; 1987

[9] G. Petzow, “Metallographisches, Keramographisches, Plastographisches Ätzen”, “Materialkundlich-Technische Reihe 1”, 6. Auflage, Gebrüder Bornträger, Berlin Stuttgart 1994, ISBN 3-443-23014-8

[10] Product page of Struers for electrolytical preparation devices: http://www.struers.at/default.asp?top_id=3&main_id=12&doc_id=208&target=_self&admin_language=2 [13.02.2015]

[11] Zankel et.al.: “Ultramicrotomy in the ESEM, a versatile method for materials and life sciences” Journal of Microscopy, Vol. 233, Pt 1 2009, pp. 140–148; Received 29 April 2008; accepted 18 July 2008

[12] Zankel et.al.: “Serial sectioning methods for 3D investigations in materials science”, Review, Elsevier, Micron 62 (2014) pp. 66–7

[13] E. Lee Bray: “Aluminum” from U.S. Geological Survey, Mineral Commodity Summaries, February 2014 http://minerals.usgs.gov/minerals/pubs/commodity/aluminum/mcs-2014-alumi.pdf (12.12.2014)

[14] F. Habaschi (Ed.), “Alloys–Preparation, Properties, Applications”, Wiley–VCH, 1998

[15] W. Weißbach: “Werkstoffkunde – Strukturen, Eigenschaften, Prüfung“, Vieweg +Teubner Verlag, Springer Fachmedien Wiesbaden GmbH, Springer Science+Business Media, 18th Edition, 2012

[16] I. De Graeve and J. Hirsch; “Classification of the Wrought Alloy Series”; Alu Matter; Wrought Aluminum alloys; Site developed in partnership between the European Aluminium Association and MATTER © 2001-2010 MATTER, The University of Liverpool http://aluminium.matter.org.uk/content/html/eng/default.asp?catid=214&pageid=2144417045 (12.12.2014)

[17] C. Kammer; „Aluminium Taschenbuch 3: Weiterverarbeitung und Anwendung“, Beuth Verlag GmbH; 17. Vollständige überarbeitete Auflage; 2014, p.12-14

[18] I. De Graeve and J. Hirsch; “2XXX Series Alloys”; Alu Matter; Wrought Aluminum alloys; Site developed in partnership between the European Aluminium Association and MATTER © 2001-2010 MATTER, The University of Liverpool http://aluminium.matter.org.uk/content/html/eng/default.asp?catid=214&pageid=2144417081 (12.12.2014)

[19] J. C. Williams et. al., “Progress in structural materials for aerospace systems”; Acta Materialia 51 (2003) 5775–5799

[20] Hüttenaluminium-Gusslegierungen, RHEINFELDEN ALLOYS, Leporello; http://www.miguss.de/upload/5729081-Leporello-Httenaluminium-Gusslegierungen-RHEINFELDEN-ALLOYS-2013-DE.pdf (12.12.2014)

[21] Universität Stuttgart; Sonderforschungsbereich 716; Beschreibung: http://www.sfb716.uni-stuttgart.de/forschung/teilprojekte/projektbereich-b/b7/beschreibung.html (12.12.2014)

[22] Micrographs: Aluminum Copper (Age Hardened); this site is designed and built by Logical Cobwebs and owned by NATEC.

http://pwatlas.mt.umist.ac.uk/internetmicroscope/micrographs/microstructures/more-metals/al-alloys/age-hardened_z3.html (12.12.2014)

[23] Prof. Dr. K. Hentschel; “Duraluminum“ Universität Stuttgart; http://www.uni-stuttgart.de/hi/gnt/ausstellungen/zeppelin/1.2_duralumin.html (12.12.2014)

[24] E. Moeller; „Handbuch Konstruktionswerkstoffe: Auswahl, Eigenschaften, Anwendung“, HANSER-Verlag, 2014, 2. Überarbeitete Auflage; p. 382 ff

[25] Y. Huang, et al., Journal of Magnesium and Alloys (2014) Volume 2, Issue 2m p. 124 – 132

[26] Shae K. Kim; “Design and Development of High-Performance Eco-Mg Alloys”, in “Magnesium Alloys - Design, Processing and Properties”, Ed. Frank Czerwinski, 2011, ISBN: 978-953-307-520-4, InTech, DOI: 10.5772/13836. Available from: http://www.intechopen.com/books/magnesium-alloys-design-processing-and-properties/design-and-development-of-high-performance-eco-mg-alloys (12.12.2014)

[27] L. Reimer et. al; “Transmission Electron Microscopy”, Springer LLC, 2008, 5th Edition

[28] D. Focosi; Microscopy, http://www.ufrgs.br/imunovet/molecular_immunology/microscopy.html, 12.12.2014

[29] Schema of a transmission electron microscope http://en.wikipedia.org/wiki/Transmission_electron_microscopy#mediaviewer/File:Scheme_TEM_en.svg (13.02.2015)

[30] F. Hofer, P. Warbichler: „EFTEM elemental mapping in materials science“, in „Transmission Electron Energy Loss Spectrometry in Materials Science and the EELS Atlas“, C.C. Ahn (Ed.). Wiley-VCH, Berlin (2004). pp.181– 233

[31] R.F. Egerton: “Electron Energy-Loss Spectroscopy in the Electron Microscope”, Springer Science and Business Media, LLC, 2011, p. 293 ff, 419

[32] Instrumentation of FELMI–ZFE http://portal.tugraz.at/portal/page/portal/felmi/instrumentation (12.12.2014)

[33] Model 1040 NanoMill® TEM specimen preparation system, by Fischione

[34] T. B. Isabell et.al.: “Plasma Cleaning and Its Applications for Electron Microscopy”, Microsc. Microanal. 5, 126-135, 1999

[35] M.J. Vasile: “A comparative study of the radio frequency discharge in gas mixtures of helium with flourine, oxygen, nitrogen, and argon”, Journal of Applied Physics 51, 2503 (1980); doi: 10.1063/1.328024

[36] Electrolyte from STRUERS from TenuPol5 device

[37] K. Teichmann et.al; TEM study of β′ precipitate interaction mechanisms with dislocations and β′ interfaces with the aluminum matrix in Al–Mg–Si alloys, Materials Characterization 75 (2013) 1–7

[38] Model 110 Automatic Twin – Jet Electropolisher Recipes (Fischione), for Al Alloy 2024

[39] A. Wiengmoon et.al., HRTEM and HAADF–STEM of precipitates at peak ageing of cast A319 aluminum alloy, Micron 45 (2013) 32–36

[40] Dr. J. Li; personal recommendation

[41] Dr. J. Li; “A precipitation Microstructure and their strengthening effects of an Mg-2.8Nd-0.6Zn-0.4Zr alloy with a 0.2 wt% addition

[42] Y. Guangyn et.al, High temperature deformation behavior of permanent casting AZ91 alloy with and without SB addition; Journal of materials Science 37 (2002) 127 - 132

[43] Y. D: Huang et.al, Evolution of microstructure and hardness of AE42 alloy after heat treatments; Journal of Alloys and Compounds 463 (2008) 238 - 145

10. Appendix

Aluminium alloys:

1. Experiment		**31.03.2014**		
Electrolyte	1		Sample	AA2016
Flowrate	13			
	Specimen	Voltage [V]	Temperature [°C]	time [m:sec]
	specimen thickness			
a	156	30	-8	00:52
b	155	35	-6	00:40
c	153	40	-5	00:16
d	150	45	-5	00:14
e	149	50	-4	00:25

2. Experiment		**01.04.2014**		
Electrolyte	1		Sample	AA2016
Flowrate	13			
	Specimen	Voltage [V]	Temperature [°C]	time [m:sec]
	specimen thickness			
a	151	5	-13	00:10
b	159	10	-10	03:16
c	160	15	-7	01:57
d	155	20	-6	01:32

3. Experiment		**03.04.2014**		
Electrolyte	1		Sample	AA2016
Flowrate	13			
	Specimen	Voltage [V]	Temperature [°C]	time [m:sec]
	specimen thickness			
a	89	15	-15	01:08
b	92	20	-11	01:04
c	91	25	-10	00:45
d	92	30	-8	00:30
e	93	35	-6	00:28

4. Experiment		**07.04.2014**		
Electrolyte	1		Sample	AA2016
Flowrate	13			
	Specimen	Voltage [V]	Temperature [°C]	time [m:sec]
	specimen thickness			
a	193	45	-14	01:56
b	189	50	-13	01:07
c	199	55	-11	00:54
d	199	60	-9	00:37

5. Experiment		14.04.2014			
Electrolyte	1	Sample	AA2016	upper gun	4°
Voltage	20	PIPS	4 keV	lower gun	6°
	Specimen	Flowrate	Temperature [°C]	time [m:sec]	PIPS [t]
	specimen thickness				
a	145	10	-13	02:24	02:00
b	156	12	-10	01:36	03:13
c	157	14	-9	01:16	
d	161	16	-8	01:26	07:00
e	144	18	-7	01:15	18:00
f	164	20	-5	01:24	11:11

6. Experiment		14.04.2014			
Electrolyte	1	Sample	AA2016	upper gun	4°
Voltage	20	PIPS	4 keV	lower gun	6°
	Specimen	Flowrate	Temperature [°C]	time [m:sec]	PIPS [t]
	specimen thickness				
a	148	10	-15	01:26	04:00
b	146	12	-13	01:16	0
c	143	14	-10	01:07	0
d	144	16	-9	00:55	0
e	148	18	-7	01:06	01:15
f	149	20	-5	00:49	01:15

7. Experiment		**23.04.2014**			
Electrolyte	1	Sample	AA2016	upper gun	4°
Flowrate	13	PIPS	4 keV	lower gun	6°
	Specimen specimen thickness	Voltage [V]	Temperature[°C]	time [m:sec]	PIPS [t]
a	149	35	-9	01:25	06:00:00
b	165	35	-7	01:08	15:30
c	172	35	-6	01:01	06:30

8. Experiment		**21.05.2014**			
Electrolyte	1	Sample	AA2016	upper gun	4°
Flowrate	13	PIPS	4 keV	lower gun	6°
	Specimen specimen thickness	Voltage [V]	Temperature [°C]	time [m:sec]	PIPS [t]
a	150	35	-23.7	09:14	07:01
b	150	35	-20.6	03:45	05:01
c	152	35	-19.8	03:48	14:00

9. Experiment		12.06.2014			
Electrolyte	1	Sample	AA2016	upper gun	4°
Flowrate	13	PIPS	4 keV	lower gun	6°

	Specimen	Voltage [V]	Temperature [°C]	time [m:sec]	PIPS [t]
	specimen thickness				
	Sample A				
a	140	35	-20.2	01:46	03:30
b	150	35	-19.5	02:44	09:10
	Sample B				
a	167	35	-20.1	03:37	03:21
b	154	35	-20.7	03:06	03:40
	Sample C				
a	149	35	-20.3	03:14	04:00
b	149	35	-20.8	02:55	21:00
	Sample D				
a	152	35	-20.4	02:33	20:00
b	162	35	-20	03:30	05:00

10. Experiment		15.07.2014				
Electrolyte	2	Sample	AA2618	upper gun	4°	
Flowrate	13	PIPS	4 keV	lower gun	6°	

	Specimen	Voltage [V]	Temperature [°C]	time [m:sec]	mA	PIPS [t]
	specimen thickness					
a	166	10	-21.5	03:54	124	
b	168	15	-19.5	03:28	216	01:30
c	160	20	-20.7	03:09	217	01:15
d	165	25	-20.8	01:28	314	
e	169	30	-19	01:27	438	
f	167	35	-20.5	01:27	470	04:00

11. Experiment		**30.07.2014**			
Electrolyte	3		Sample	AA2618	
Flowrate	13				
	Specimen	Voltage [V]	Temperature [°C]	time [m:sec]	mA
	specimen thickness				
a	167	10	-21.3	06:51	34
b	171	15	-19.4	02:57	55
c	168	20	-20.1	01:44	92
d	172	25	-21.5	01:49	118
e	172	30	-21.7	01:30	153
f	160	35	-21.2	00:49	196

12. Experiment		**03.09.2014**			
Electrolyte	3		Sample	AA2016	
Flowrate	13				
	Specimen	Voltage [V]	Temperature [°C]	time [m:sec]	mA
	specimen thickness				
a	154	10	-19.7	05:29	47
b	147	15	-19.9	02:36	81
c	145	20	-20	01:49	120
d	164	25	-20.1	02:31	120
e	154	30	-20.3	01:45	150
f	159	35	-20.3	01:44	190

13. Experiment		**14.10.2014**			
Electrolyte	4		Sample	AA2618	
Flowrate	13				
	Specimen	Voltage [V]	Temperature [°C]	time [m:sec]	mA
	specimen thickness				
a	160	15	-21.9	01:33	72
b	156	20	-22.4	01:20	94
c	144	25	-22.8	01:07	116
d	157	30	-23	00:49	142
e	148	35	-23.1	00:52	164
f	160	40	-23	00:46	195

14. Experiment		**20.10.2014**			
Electrolyte	3		Sample	AA2618	
Flowrate	13				
	Specimen	Voltage [V]	Temperature [°C]	time [m:sec]	mA
	specimen thickness				
a	151	23	-19.7	02:16	123
b	153	25	-19	02:04	120
c	154	28	-21.2	02:27	137
d	154	30	-21.9	02:13	150
e	152	33	-20.9	02:16	178
f	150	35	-19.5	02:08	184
g	155	38	-20.9	01:46	196
h	162	40	-20.4	02:06	203

15. Experiment		20.10.2014			
Electrolyte	3		Probe	AlCu4Ti0,2	
Flowrate	13				
	Specimen	Voltage [V]	Temperature [°C]	time [m:sec]	mA
	specimen thickness				
a	170	20	-20	04:10	96
b	157	23	-19.5	01:45	115
c	144	25	-20.2	02:52	120
d	159	27	-19.9	02:00	130
e	160	30	-20.4	03:51	144
f	141	32	-21.2	01:24	126
g	166	35	-20.5	02:20	155

TenuPol5 Paramter with AA2016:

Experiment 1 - 4

Voltage (V) / -9°C	Hole size (µm)
5	0
10	50
15	50
20	100
25	80
30	50
35	75
40	200
45	125
50	100
55	40
60	45

Experiment 5 and 6

Flowrate (ml/s) / -9°C	at 20 V	at 35 V
10	50	50
12	50	35
14	75	100
16	50	75
18	50	60
20	45	75

Eco AM50 preparation:

1. Experiment	**05.05.2014**		
Electrolyte	1	Sample	Eco AM 50
Current	24 V		
Specimen	Flowrate	Temperature [°C]	time [m:sec]
specimen thickness			
a 152	10	22	01:16
b 154	12	22	00:52
c 150	14	22	01:15
d 153	16	22	00:52
e 154	18	22	00:56
f 151	20	22	00:52

2. Experiment		07.05.2014		
Electrolyte		2	Probe	Eco AM50
Current		20 V		
	Specimen	Flowrate	Temperature [°C]	time [m:sec]
	specimen thickness			
a	152	10	-15	00:13
b	157	12	-15	00:13
c	148	14	-13	00:10
d	147	16	-11	00:09
e	145	18	-10	00:09
f	166	20	-10	00:09

3. Experiment		07.05.2014			
Electrolyte	1	Probe	Eco AM50	upper gun	4°
Flowrate	13	PIPS	4 kev	lower gun	6°
	Specimen	Voltage [V]	Temperature [°C]	time [m:sec]	PIPS [t]
	specimen thickness				
a		24	-38	05:03	01:23:05
b		24	-37.2	03:30	
c		24	-37	03:43	0:40:00
d		24	-37	04:10	03:30:00

4. Experiment		26.06.2014			
Electrolyte	2		Sample	Eco AM50	
Flowrate	13				
	Specimen specimen thickness	Voltage [V]	Temperature [°C]	time [m:sec]	mA
a	151	20	-41.5	01:33	170
b	155	20	-40.9	02:10	150
c	151	20	-40.3	02:15	170
d	160	20	-40.2	02:58	150
e	145	20	-40.8	02:36	150

5. Experiment		15.07.2014			
Electrolyte	3		Sample	Eco AM50	
Flowrate	13				
	Specimen specimen thickness	Voltage [V]	Temperature [°C]	time [m:sec]	mA
a	148	10	-37.9	03:20	74
b	145	15	-38	02:22	130
c	146	20	-38	02:39	180
d	151	25	-38	01:54	218
e	150	30	-37.4	01:42	278
f	156	35	-37.4	01:06	360

6. Experiment		**30.07.2014**			
Electrolyte	4		Sample	Eco AM50	
Flowrate	13				
	Specimen	Voltage [V]	Temperature [°C]	time [m:sec]	mA
	specimen thickness				
a	163	10	-40	04:25	32
b	168	15	-40,5	02:27	50
c	159	20	-40,2	02:06	63
d	160	25	-40,1	01:38	82
e	166	30	-40,1	01:34	94
f	159	35	-40	01:24	120

7. Experiment		**06.08.2014**			
Electrolyte	5		Sample	Eco AM50	
Flowrate	13				
	Specimen	Voltage [V]	Temperature [°C]	time [m:sec]	mA
	specimen thickness				
a	124	10	-30.3	04:42	12
b	146	15	-30.8	05:10	18
c	152	20	-31.3	02:37	24
d	132	10	-39.6	08:40	10
e	150	15	-40	06:32	14
f	145	20	-40.2	07:28	18

8. Experiment	**27.08.2014**				
Electrolyte	6		Probe	Eco AM50	
Flowrate	13				
	Specimen	Voltage [V]	Temperature [°C]	time [m:sec]	mA
	specimen thickness				
a	154	25	-29	03:56	23
b	153	30	-30	04:46	27
c	147	35	-30.4	03:42	28
d	147	40	-30.9	03:33	37
e	150	45	-31.3	03:15	38